USGS
science for a changing world

2016 One-Year Seismic Hazard Forecast for the Central and Eastern United States from Induced and Natural Earthquakes

By Mark D. Petersen, Charles S. Mueller, Morgan P. Moschetti, Susan M. Hoover, Andrea L. Llenos, William L. Ellsworth, Andrew J. Michael, Justin L. Rubinstein, Arthur F. McGarr, and Kenneth S. Rukstales

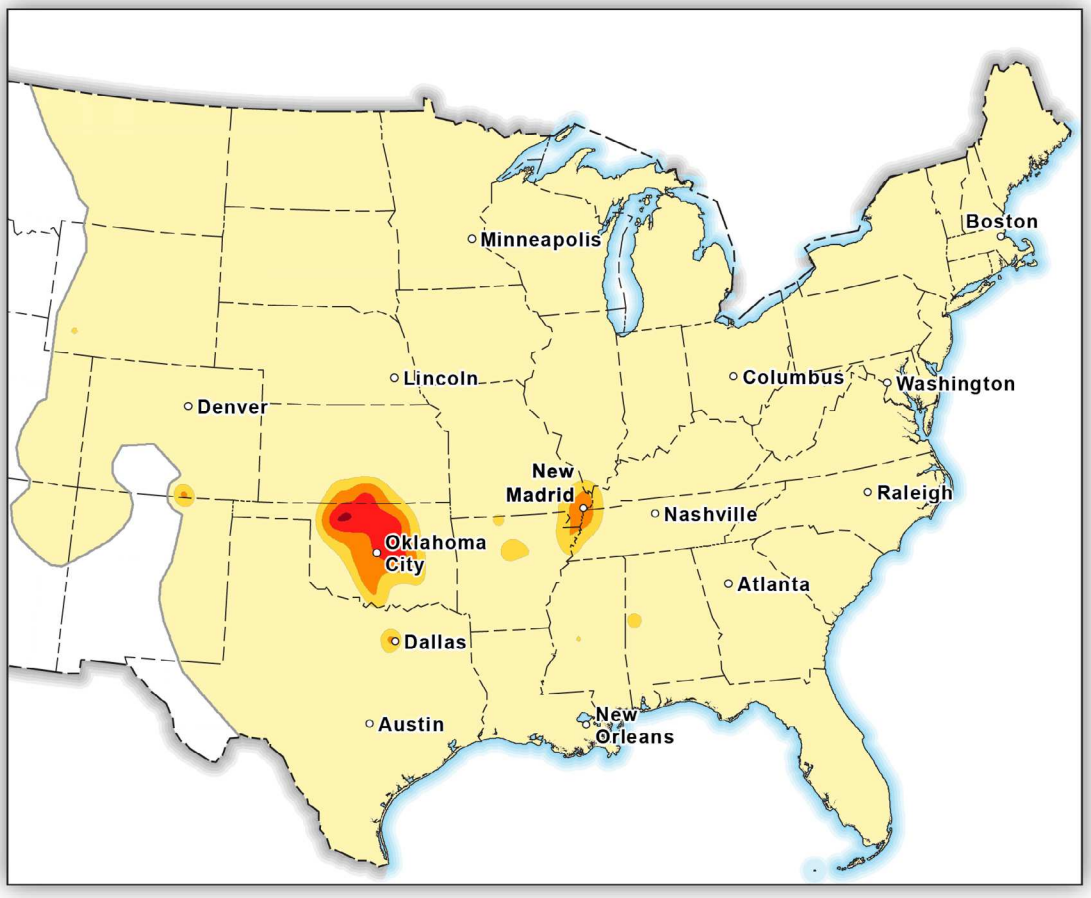

Open-File Report 2016–1035

U.S. Department of the Interior
U.S. Geological Survey

U.S. Department of the Interior
SALLY JEWELL, Secretary

U.S. Geological Survey
Suzette M. Kimball, Director

U.S. Geological Survey, Reston, Virginia: 2016

For more information on the USGS—the Federal source for science about the Earth, its natural and living resources, natural hazards, and the environment—visit http://www.usgs.gov/ or call 1–888–ASK–USGS (1–888–275–8747).

For an overview of USGS information products, including maps, imagery, and publications, visit http://www.usgs.gov/pubprod/.

Any use of trade, firm, or product names is for descriptive purposes only and does not imply endorsement by the U.S. Government.

Although this information product, for the most part, is in the public domain, it also may contain copyrighted materials as noted in the text. Permission to reproduce copyrighted items must be secured from the copyright owner.

Suggested citation:
Petersen, M.D., Mueller, C.S., Moschetti, M.P., Hoover, S.M., Llenos, A.L., Ellsworth, W.L., Michael, A.J., Rubinstein, J.L., McGarr, A.F., and Rukstales, K.S., 2016, 2016 One-year seismic hazard forecast for the Central and Eastern United States from induced and natural earthquakes: U.S. Geological Survey Open-File Report 2016–1035, 52 p., http://dx.doi.org/10.3133/ofr20161035.

ISSN 2331-1258 (online)

Cover: Map showing chance of damage from an earthquake in the Central and Eastern United States during 2016. Percent chances are represented as follows: pale yellow, less than 1 percent; dark yellow, 1 to 2 percent; orange, 2 to 5 percent; red, 5 to 10 percent; dark red, 10 to 12 percent.

Acknowledgments

We wish to thank the November 2014 Induced Seismicity workshop participants, over 100 individuals who made valuable suggestions for revising the 2014 U.S. Geological Survey (USGS) National Seismic Hazard Modeling Project maps and models to incorporate induced seismicity. We thank State geological survey representatives and experts on induced seismicity from Alabama, Arkansas, Colorado, Kansas, New Mexico, Ohio, Oklahoma, and Texas for their guidance in delineating and discussing potential induced seismicity zones. In particular, we would like to thank Scott Ausbrooks, Karen Berry, Lisa Block, Jeremy Boak, Rex Buchanan, Amberlee Darold, Heather DeShon, Sandy Ebersole, Jeff Fox, Cliff Frohlich, Michael Hansen, Austin Holland, Matt Hornbach, Steve Horton, Dave Love, Thomas Serenko, Nick Tew, Scott Tinker, and Lynn Watney for providing extensive comments and review. We also thank members of the National Seismic Hazard and Risk Assessment Steering Committee—John Anderson (chair), Norm Abrahamson, Kenneth Campbell, Martin Chapman, Michael Hamburger, William Lettis, Nilesh Shome, Ray Weldon, and Chris Wills—who reviewed the documentation, data, methods, and models, and provided important feedback that helped us to improve the quality of this product. In addition, we thank Dan McNamara for reviewing the document. We thank the USGS Earthquake Hazard Program for funding the development of the maps. This work benefited from discussions with Robert Williams, Jill McCarthy, David Wald, Bruce Worden, Vince Quitoriano, Kishor Jaiswal, Michael Blanpied, and Harley Benz. We thank Melanie Parker and Mari Kauffmann for editing the manuscript and figures. We also thank Kristi Hartley, Tania Larson, and Janet Slate for facilitating the publication of this report.

Contents

Abstract 1
Introduction 1
Classification of Induced and Natural Earthquakes 12
Seismic Hazard Models Including Induced and Natural Earthquakes in the CEUS 14
  Methodology 14
  Model Development: Logic Tree for Sources Within Induced Zones (Figure 3*A*) 17
    Level 1: Catalog and Earthquake Sources 17
    Level 2: Alternative Models for Classifying Induced and Natural Earthquakes 17
    Level 3: Earthquake Catalog Duration 18
      Informed Model 18
      Adaptive Model 18
    Level 4: Smoothing Distances Applied in Predictive Model 18
    Level 5: Maximum Magnitude (Mmax) 19
    Level 6: Ground Motion Models 19
  Model Development: Logic Tree for Sources Outside of Induced Zones (Figure 3*B*) 20
Results 20
  Seismic Hazard Maps 20
  Hazard Curves 32
  Modified Mercalli Intensity Maps 34
  Final Maps 37
Conclusions 40
References 41
Appendix 1. Likelihood Testing for Smoothed Seismicity Parameters, Oklahoma and Southern Kansas 48
Appendix 2. The Adaptive Model 50

Figures

1. Zones of induced seismicity defined in this report, information on oil and gas plays, sedimentary basins (U.S. Energy Information Administration, 2015), wells that are associated with earthquakes (Weingarten and others, 2015), and the earthquake rate from 1980 through 2015 in the Central and Eastern United States 6
2. Seismicity maps of the earthquake catalogs used to assess the 2016 hazard across the Central and Eastern United States 8
3. Two logic trees applied in the 2016 one-year seismic hazard model 15
4. Peak horizontal ground acceleration hazard maps showing sensitivity to input parameters relative to a base case 22
5. Comparisons of the hazard maps 1-percent probability of exceedance in 1 year for adaptive and informed models and for the final model and the 2014 National Seismic Hazed Model 28
6. Peak horizontal ground acceleration hazard curves for towns and cities located near induced earthquakes for the 2016 one-year model and for the 2014 National Seismic Hazard Model 33

7. Modified Mercalli Intensity maps and chance of damage for the Western United States and the Central and Eastern United States based on peak horizontal ground acceleration and 1-hertz spectral acceleration 35
8. Final hazard maps for Modified Mercalli Intensity (MMIs) and chance of damage for the Western United States and the Central and Eastern United States based on averages of MMIs converted from peak horizontal ground acceleration and 1-hertz spectral acceleration 38
1–1. Information gains and optimized smoothing distances as a function of the catalog year of the events used to develop trial smoothed seismicity models 49
2–1. Maps showing maximum earthquake rates from the 1-year, 2-year, 36-year, and 2014 National Seismic Hazard Model long-term catalogs, and a seismicity map 51
2–2. Maps comparing trimmed and untrimmed earthquake rates 52

Tables

1. Zones of induced seismicity considered in this assessment 3
2. Regions of induced seismicity to consider in the future 11

2016 One-Year Seismic Hazard Forecast for the Central and Eastern United States from Induced and Natural Earthquakes

By Mark D. Petersen, Charles S. Mueller, Morgan P. Moschetti, Susan M. Hoover, Andrea L. Llenos, William L. Ellsworth, Andrew J. Michael, Justin L. Rubinstein, Arthur F. McGarr, and Kenneth S. Rukstales

Abstract

The U.S. Geological Survey (USGS) has produced a 1-year seismic hazard forecast for 2016 for the Central and Eastern United States (CEUS) that includes contributions from both induced and natural earthquakes. The model assumes that earthquake rates calculated from several different time windows will remain relatively stationary and can be used to forecast earthquake hazard and damage intensity for the year 2016. This assessment is the first step in developing an operational earthquake forecast for the CEUS, and the analysis could be revised with updated seismicity and model parameters. Consensus input models consider alternative earthquake catalog durations, smoothing parameters, maximum magnitudes, and ground motion estimates, and represent uncertainties in earthquake occurrence and diversity of opinion in the science community. Ground shaking seismic hazard for 1-percent probability of exceedance in 1 year reaches 0.6 g (as a fraction of standard gravity [g]) in northern Oklahoma and southern Kansas, and about 0.2 g in the Raton Basin of Colorado and New Mexico, in central Arkansas, and in north-central Texas near Dallas. Near some areas of active induced earthquakes, hazard is higher than in the 2014 USGS National Seismic Hazard Model (NHSM) by more than a factor of 3; the 2014 NHSM did not consider induced earthquakes. In some areas, previously observed induced earthquakes have stopped, so the seismic hazard reverts back to the 2014 NSHM. Increased seismic activity, whether defined as induced or natural, produces high hazard. Conversion of ground shaking to seismic intensity indicates that some places in Oklahoma, Kansas, Colorado, New Mexico, Texas, and Arkansas may experience damage if the induced seismicity continues unabated. The chance of having Modified Mercalli Intensity (MMI) VI or greater (damaging earthquake shaking) is 5–12 percent per year in north-central Oklahoma and southern Kansas, similar to the chance of damage caused by natural earthquakes at sites in parts of California.

Introduction

The 2014 U.S. Geological Survey (USGS) United States National Seismic Hazard Model (NSHM) provides forecasts of locations, magnitudes, and rates of future natural (tectonic) earthquakes, as well as estimates of long-term ground shaking hazard that are applied in building codes and site-specific structural designs, risk assessments, financial instruments, and other public policy applications (Petersen and others, 2014, 2015a). As in previous hazard models, nontectonic events were removed from consideration in the 2014 hazard assessment, so that model does not consider mining-related seismicity or earthquakes caused by wastewater injection or other human activities.

In this report, referring to earthquakes and seismicity as "induced" or "potentially induced" indicates that the seismicity in a given region has shown an increased earthquake rate that can be attributed to human activities, such as fluid injection or extraction (Segall, 1989; Segall and Lu, 2015). We acknowledge that this classification is based on circumstantial evidence and scientific judgment and that a lack of relevant technical information on the geological condition, state of stress, and human industrial activity (such as injection well pumping data) makes it difficult to assess seismic hazard. In this report, however, we do not explore the causes of the increased seismicity, but rather we try to find a way to quantify the associated hazard. Because regions of induced seismicity are identified by sharp increases in the rate of earthquakes in a particular area, we consider induced earthquakes to be earthquakes within a certain area and time window that have been provisionally identified by the science literature and local expertise.

Earthquake rates have recently increased markedly in multiple areas of the Central and Eastern United States (CEUS), especially since 2010, and scientific studies have linked the majority of this increased activity to wastewater injection in deep disposal wells (table 1) (Ellsworth, 2013; Keranen and others, 2014; Walsh and Zoback, 2015; Weingarten and others, 2015). Figure 1 shows the location of wells associated with earthquakes (Weingarten and others, 2015) and a timeline of earthquake rates, and figure 2 shows the seismicity maps for varying time intervals in the CEUS. Between 1980 and about 2010, CEUS earthquake rates were relatively stable, but recent rates in some areas have increased by more than an order of magnitude. Such changes have caused concern to many, including residents, business owners, engineers, and public officials responsible for mitigating or responding to the effects of these earthquakes on nearby populations (for example, Ground Water Protection Council and Interstate Oil and Gas Compact Commission, 2015).

Table 1. Zones of induced seismicity considered in this assessment. For each zone, weight, earthquake rates, time windows, and data sources are shown.

[Spanner colors correspond with label colors used in figures 1 and 2. See text for details on unresolved zones. Weight given as decimal percentage. M, adjusted moment magnitude; dec., declustered earthquake catalog; full, non-declustered earthquake catalog]

Zones of induced seismicity	Weight based on scientific consensus—considered induced	1-year count M2.7+ through fall 2015		2-year count M2.7+ through fall 2015		Start year–end year (if applicable)	Largest earthquake (M, date)	References
		dec.	full	dec.	full			
Zones that have had M2.7 and greater earthquake activity in years 2014–2015								
Greeley, Colorado	1.0—yes	0	0	1	1	2013–present	3.2, Jun. 2014	Yeck and others (2014), Ground Water Protection Council and Interstate Oil and Gas Compact Commission (2015, appendix C)
Youngstown, Ohio	1.0—yes	0	0	1	2	2010–present	3.7, Dec. 2011	Kim (2013), Skoumal and others (2015a, b)
Oklahoma-Kansas	1.0—yes	149	3,528	292	5,991	2006–present	5.6, Nov. 2011	Keranen and others (2013, 2014), Sumy and others (2014), Andrews and Holland (2015), Buchanan (2015), Walsh and Zoback (2015)
Cogdell, Texas	1.0—yes	1	1	3	4	1976–present	4.5, Jun. 1978	Davis and Pennington (1989), Gan and Frohlich (2013)
Fashing, Texas	1.0—yes	1	1	2	2	1973–present	4.6, Oct. 2011	Pennington and others (1986), Frohlich and Brunt (2013)
North Texas (Azle, Cleburne area, Dallas-Fort Worth Airport, Mineral Wells)	1.0—yes	0	0	1	1	2008–present	3.4, Nov. 2013	Frohlich and others (2011), Frohlich (2012), Justinic and others (2013), Hornbach and others (2015)
Timpson, Texas	1.0—yes	0	0	1	1	2011–present	4.8, May 2012	Frohlich and others (2014)
Venus, Texas	1.0—yes	1	1	2	2	2008–present	4.0, May 2015	Frohlich (2012)

Table 1. Zones of induced seismicity considered in this assessment. For each zone, weight, earthquake rates, time windows, and data sources are shown.—Continued

[Spanner colors correspond with label colors used in figures 1 and 2. See text for details on unresolved zones. Weight given as decimal percentage. M, adjusted moment magnitude; dec., declustered earthquake catalog; full, non-declustered earthquake catalog]

Zones of induced seismicity	Weight based on scientific consensus—considered induced	1-year count M2.7+ through fall 2015		2-year count M2.7+ through fall 2015		Start year–end year (if applicable)	Largest earthquake (M, date)	References
		dec.	full	dec.	full			
Zones that have not had M2.7 and greater earthquake activity in years 2014–2015								
El Dorado, Arkansas	1.0—yes	0	0	0	0	1983–present	2.9, Jun. 1994	Cox (1991)
Paradox Valley, Colorado	1.0—yes	0	0	0	0	1991–present	3.9, Jan. 2013	Ake and others (2005), King and others (2014), Block and others (2014, 2015), Yeck and others (2015)
Rangely, Colorado-Utah	1.0—yes	0	0	0	0	1957–present	4.3, Apr. 1970	Raleigh and others (1976), Karen A. Berry, Colorado Geological Survey, written commun. (2015)
Rocky Mountain Arsenal, Colorado	1.0—yes	0	0	0	0	1962–1979	4.8, Aug. 1967	Evans (1966), Healy and others (1968), Karen A. Berry, Colorado Geological Survey, written commun. (2015)
Dagger Draw, New Mexico	1.0—yes	0	0	0	0	1998–present	4.1, Dec. 2005	Sanford and others (2006), Pursley and others (2013)
Ashtabula, Ohio	1.0—yes	0	0	0	0	1987–2007	3.9, Jan. 2001	Seeber and others (2004)
Perry, Ohio	1.0—yes	0	0	0	0	1975–present	4.6, Jan. 1986	Nicholson and others (1988), Skoumal and others (2015a)
Alice, Texas	1.0—yes	0	0	0	0	1938–present	3.5, Apr. 2010	Frohlich and others (2012)

Table 1. Zones of induced seismicity considered in this assessment. For each zone, weight, earthquake rates, time windows, and data sources are shown.—Continued

[Spanner colors correspond with label colors used in figures 1 and 2. See text for details on unresolved zones. Weight given as decimal percentage. M, adjusted moment magnitude; dec., declustered earthquake catalog; full, non-declustered earthquake catalog]

Zones of induced seismicity	Weight based on scientific consensus—considered induced	1-year count M2.7+ through fall 2015		2-year count M2.7+ through fall 2015		Start year–end year (if applicable)	Largest earthquake (M, date)	References
		dec.	full	dec.	full			
Unresolved zones								
Brewton, Alabama	0.5—partially	0	0	0	0	1997–present	4.7, Oct. 1997	Gomberg and Wolf (1999), Berry H. (Nick) Tew, Jr., Geological Survey of Alabama, written commun. (2015)
North-central Arkansas	0.8—partially	4	5	10	11	2009–present	4.7, Feb. 2011	Horton (2012), Scott Ausbrooks, Arkansas Geological Survey, written commun. (2015)
Raton Basin, Colorado-New Mexico	0.8—partially	6	10	11	18	2001–present	5.2, Aug. 2011	Meremonte and others (2001), Rubinstein and others (2014), Karen A. Berry, Colorado Geological Survey, written commun. (2015)
Sun City, Kansas	0.5—partially	2	3	2	3	2015–present	4.0, May 2015	Rex Buchanan and Lynn Watney, Kansas Geological Survey, written commun. (2015)
Irving, Texas	0.0—pending relevant published study	5	8	6	9	2008–present	3.3, Jan. 2015	Research ongoing

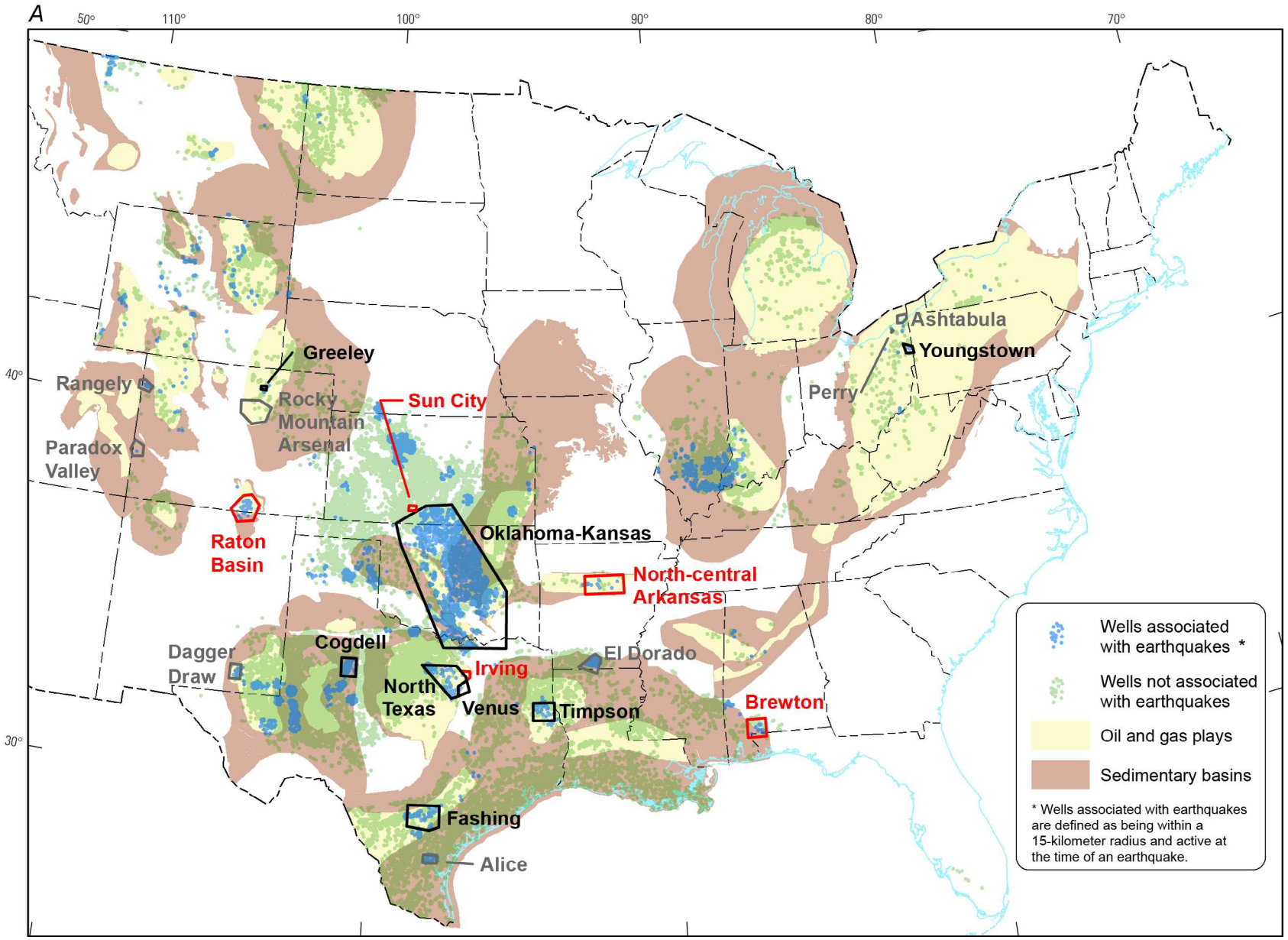

Figure caption starts on the following page.

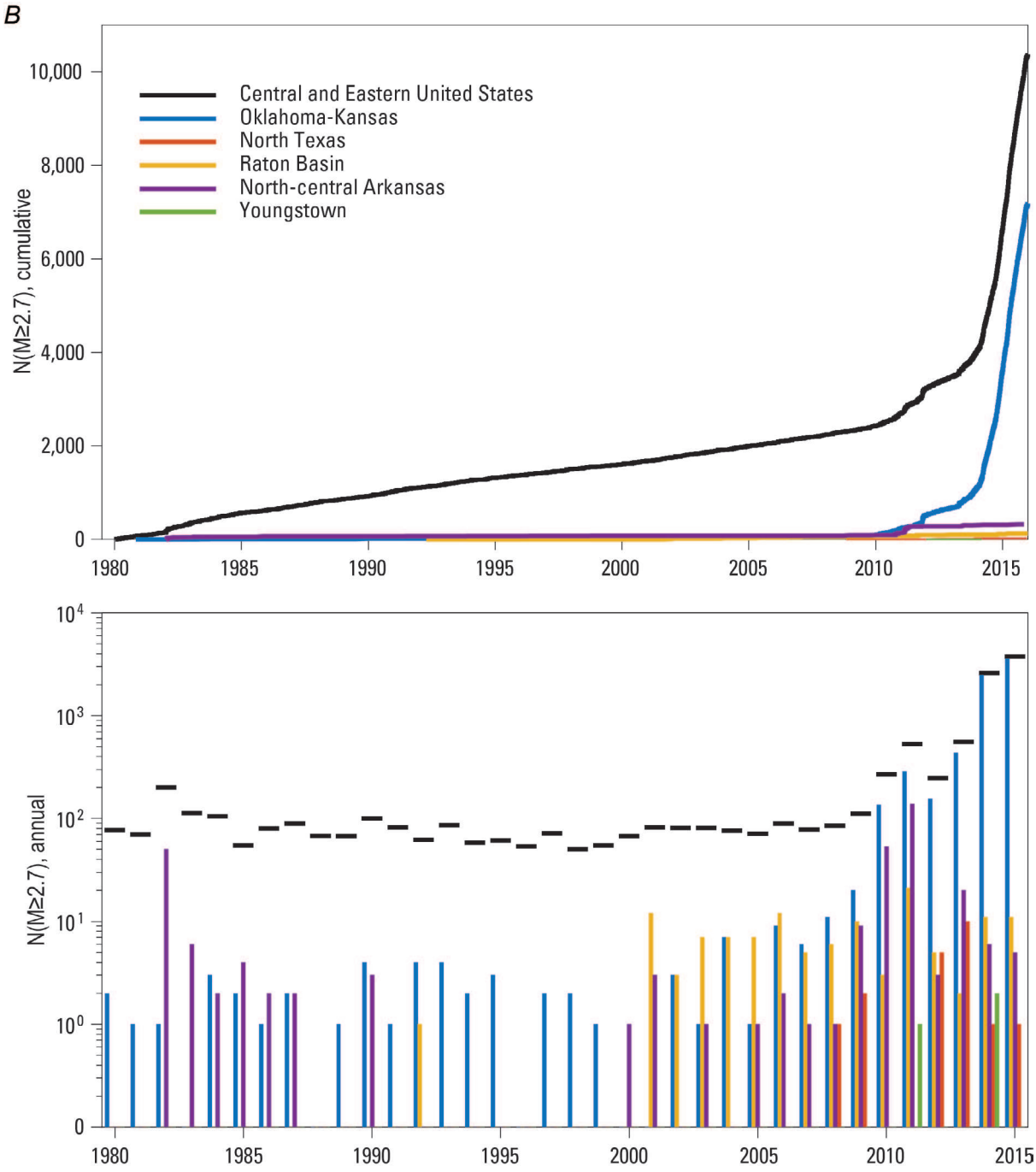

Figure 1. Zones of induced seismicity defined in this report, information on oil and gas plays, sedimentary basins, wells that are associated with earthquakes, and the earthquake rate from 1980 through 2015 in the Central and Eastern United States. *A*, Map showing locations of oil and gas plays and sedimentary basins in relation to wells that have been associated with induced seismicity (U.S. Energy Information Administration, 2015; Weingarten and others, 2015). Label colors correspond with colors used in table 1: black text identifies zones of induced seismicity that had moment magnitude (M) 2.7 and greater earthquake activity in years 2014–2015, gray text identifies zones that did not have M2.7 and greater earthquake activity in years 2014–2015, and red text identifies unresolved zones (see text for details). *B*, Cumulative (top) and annual counts (bottom) of M2.7 and greater

earthquakes in the Central and Eastern United States (CEUS) and five select zones of induced seismicity since 1980. The North Texas zone excludes Irving and Venus (fig. 1*A*, table 1). Earthquake rates are computed for this magnitude and time period (starting in 1980) because this is the earliest time for which data on M2.7 earthquakes are estimated to be complete across the region (Petersen and others, 2014).

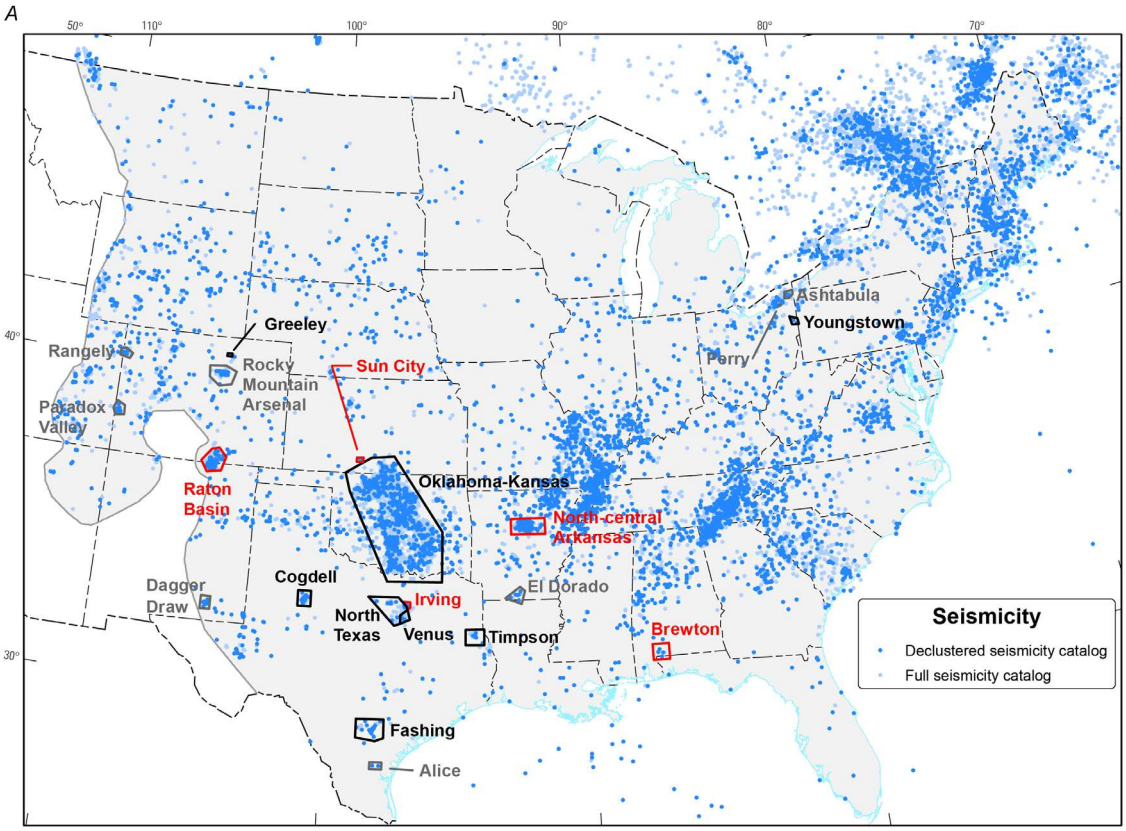

Figure caption on page 10.

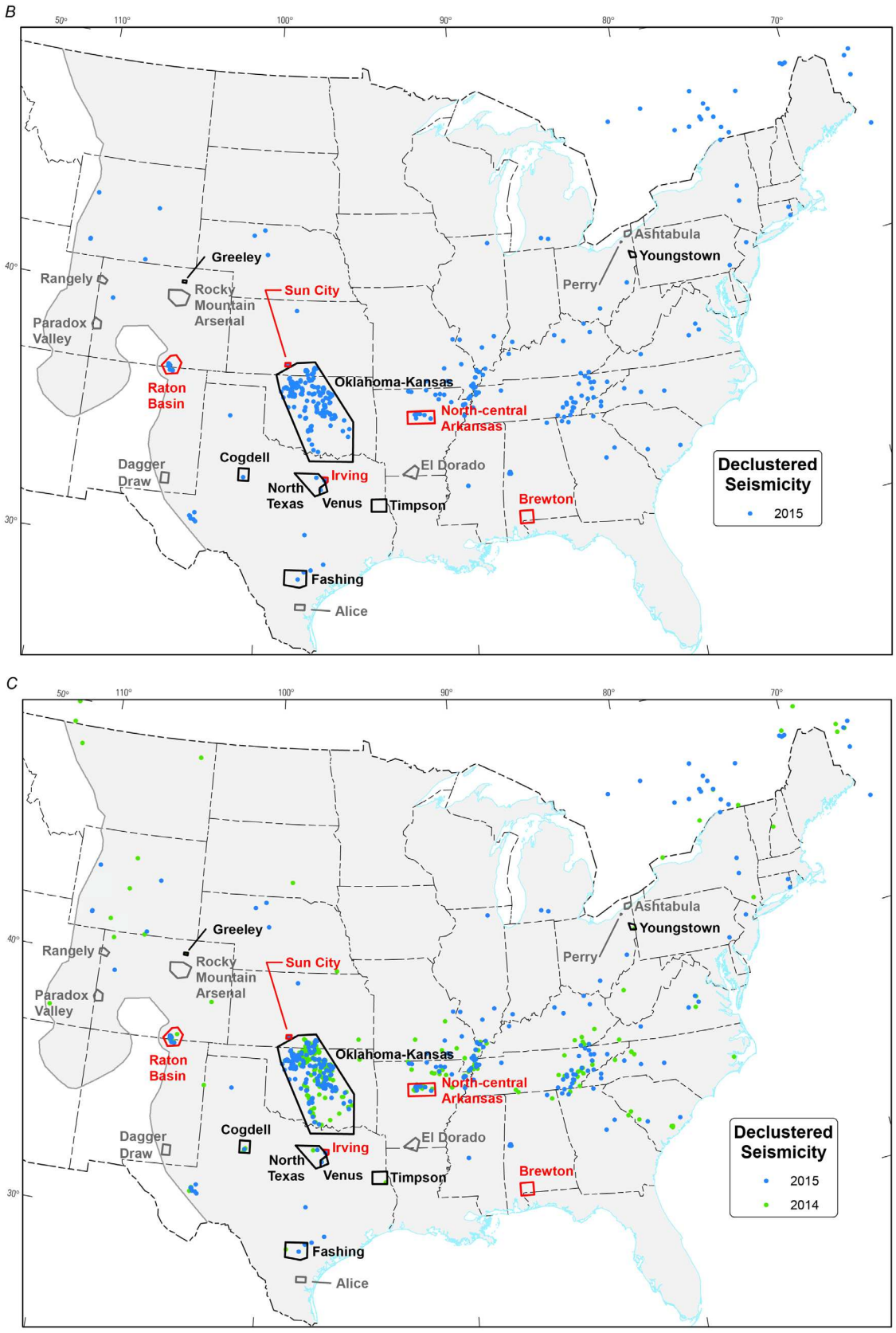

Figure caption on page 10.

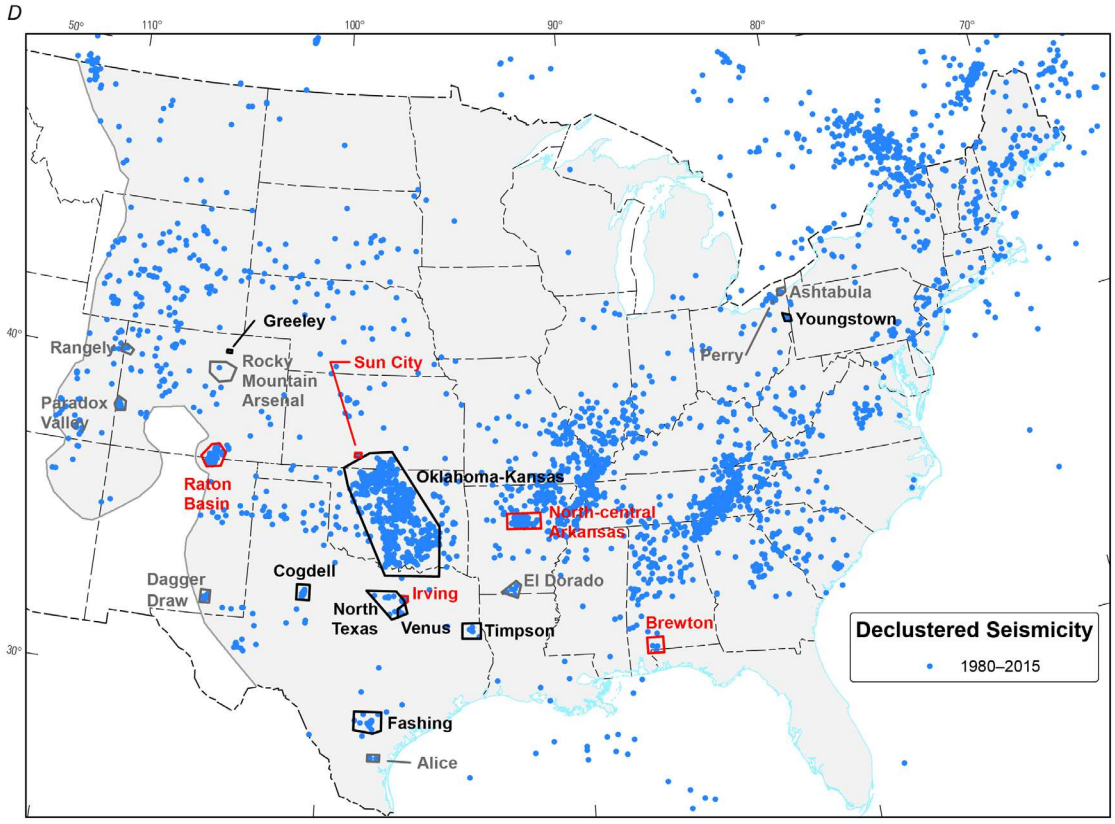

Figure 2. Seismicity maps of the earthquake catalogs used to assess the 2016 hazard across the Central and Eastern United States (CEUS; gray line indicates western boundary from 2014 National Seismic Hazard Model). Label colors correspond with colors used in table 1: black text identifies zones of induced seismicity that had moment magnitude (M) 2.7 and greater earthquake activity in years 2014–2015, gray text identifies zones that did not have M2.7 and greater earthquake activity in years 2014–2015, and red text identifies unresolved zones (see text for details). These maps show catalog durations that were applied in this assessment. *A*, Seismicity map showing the 2014 National Seismic Hazard Model's long-term catalog; earthquakes are shown for the full and declustered catalogs. *B*, Declustered seismicity map for the year 2015. *C*, Declustered seismicity map for the years 2014 and 2015. *D*, Declustered seismicity map for the years 1980 through 2015.

Assessing hazard and potential damage from these events is difficult because induced earthquakes can vary rapidly in time and space based on changes in industrial activity, which can be caused by economic or policy decisions; this variability also makes induced earthquake hazard difficult to forecast. For this reason, hazard estimates from induced earthquakes are not compatible with estimates of long-term seismic hazard caused by tectonic processes. Building-code committees are reluctant to consider induced seismicity in their current design codes because the hazard from induced earthquakes will change before the building regulations are enacted, which causes confusion in the design process. Conversely, officials will not be able to rely on standard building codes when making decisions regarding the mitigation of damage from induced earthquakes.

Even though induced earthquakes are not considered in building-code maps, they create seismic hazard to buildings, bridges, pipelines, and other important structures and are a concern for about 7.9 million people living in the vicinity of these events. Several damaging earthquakes have occurred recently near injection wells, for example, in 2011 near Prague, Oklahoma (moment magnitude [M] 5.6;

Keranen and others, 2013); in 2011 near Trinidad, Colorado (M5.3; Rubinstein and others, 2014); in 2012 near Timpson, Texas (M4.8; Frohlich and others, 2014); and in 2011 near Guy, Arkansas (M4.7; Horton, 2012). High peak accelerations have also been recorded in recent events located near active injection wells. For example, a 25 January 2013 local magnitude (mbLg) 4.1 earthquake near Timpson, Tex., caused 0.62 g (as a fraction of standard gravity [g]) peak horizontal ground acceleration (PGA) (Frohlich and others, 2014); a 10 October 2015 M4.3 earthquake near Cushing, Okla., produced 0.60 g PGA (McNamara and others, 2015b); and a 01 January 2016 M4.2 earthquake near Edmond, Okla., generated 0.58 g PGA (U.S. Geological Survey, 2016a). While peak acceleration ground shaking values may not correlate as well as peak ground velocity or other measures with damage (Worden and others, 2010), these examples illustrate that high ground shaking is occurring at sites near wastewater disposal wells.

To ascertain the best data, methods, models, and products for assessing and communicating seismic hazard from these induced earthquakes, we held a workshop in Midwest City, Okla., in November 2014 attended by more than 150 representatives from academia, government, and industry. One key issue discussed at the workshop involved the appropriate duration of the hazard forecast. It was decided that because induced earthquakes can vary so rapidly in space and time, the hazard model should only be used to forecast short intervals, such as one year, unlike the 2014 NSHM which applies a 50-year time window. A feature of a short-term forecast is that it allows for changes and could be updated annually, or even more often, if needed. Workshop participants also recommended research directions and products that would be helpful in making decisions about these earthquakes. The workshop results were summarized, research prioritized, and hazard evaluated in a report that shows sensitivity to the seismic hazard input parameters (Petersen and others, 2015b).

For this report, we built on the sensitivity study of Petersen and others (2015b) to develop a 1-year hazard model for 2016 that includes both natural and induced earthquakes within the CEUS. The model is based on geological and seismological data (fig. 2) and considers the locations of oil and gas plays and sedimentary basins (U.S. Energy Information Administration, 2015) and wells (Weingarten and others, 2015) (fig. 1*A*). The seismic hazard assessment for induced seismicity considered seismicity patterns, earthquake rates, and ground shaking data. We have delineated zones of induced seismicity (referred to as zones in this report; see table 1) based on these data and scientific literature on places where induced earthquakes are occurring. We have identified several regions of induced earthquake activity that were not included in this analysis (table 2).

Table 2. Regions of induced seismicity to consider in the future.

Region	Reference
Coso region, California	Feng and Lees (1998)
The Geysers, California	Eberhart-Phillips and Oppenheimer (1984), Oppenheimer (1986)
Salton Trough, California	Brodsky and Lajoie (2013), Wei and others (2015)
Los Angeles Basin, California	Hauksson and others (2015)
Sleepy Hollow, Nebraska	Rothe and Lui (1983)
Rattlesnake Canyon, New Mexico	Sanford and others (1993)
Bakken Shale, Montana-North Dakota	Frohlich and others (2015)
Belmont/Guernsey County, Ohio	Skoumal and others (2015a)
Harrison County, Ohio	Friberg and others (2014), Skoumal and others (2015a)
Washington County, Ohio	Skoumal and others (2015a)
Permian Basin, Texas-New Mexico	Wesson and Nicholson (1987)

To generate this model, we have held discussions with many scientists and engineers from national, State, and local government agencies; industry; and academia to define data, methods, and models that are most applicable for assessing induced earthquake hazard. This model was also discussed and reviewed by our National Seismic Hazard and Risk Assessment Steering Committee, which is composed of hazard experts from across the United States. Results of these discussions led to the following considerations. We have included two methods (an informed model and an adaptive model) to account for induced and natural earthquakes in the 2016 one-year model. Zones of induced seismicity were identified and weighted according to scientific literature and expert opinion. Those zones for which the scientific research is not yet complete (such as the Irving, Tex., zone, table 1) were not included as induced earthquakes in the model at this time as advised by local experts.

We have not included an induced earthquake hazard component for the Western United States, though studies have been done in the area. Hauksson and others (2015) attempted to identify new induced earthquakes in the Los Angeles Basin, but though they did not find widespread evidence for significant earthquake rate changes in this region, they identified two areas which may have induced activity. Several researchers (Eberhart-Phillips and Oppenheimer, 1984; Oppenheimer, 1986; Smith and others, 2000) indicated that some seismicity near the Geysers, California, may be induced. Several researchers (Brodsky and Lajoie, 2013; Wei and others, 2015) discussed indirect relationships between fluid injection activities and the triggering of two strike-slip shocks with magnitudes larger than M5.3 near Brawley, Calif., in the Salton Trough. These areas could be considered in future assessments but were not considered here. Because we consider the 2016 one-year hazard model only for the CEUS in this report, figures that include maps for the Western United States do so only for comparison. They use the 2014 NSHM based on natural earthquakes and are positioned alongside but separate from the CEUS maps.

Our assessment of induced earthquake hazard was dependent on the assumption that past earthquake rates will remain constant over the next year of the forecast. While this assumption will not hold for areas of injection over long periods, recent studies (Llenos and others, 2015; appendix 1) indicate that assessing earthquake rates observed over short time windows of a year or less are currently the best method available for forecasting the next year's rate of induced earthquakes. This model, however, does not account for increased, reduced, or new induced activity in 2016.

This assessment is the first step in developing an operational earthquake forecast for the CEUS, and the model could be updated every year, or even over a shorter time period (contingent on public interest and programmatic resources). Further research, however, is needed to ensure a robust forecasting model. For example, we considered alternative source and ground motion models for this assessment because the science of induced earthquakes is still evolving and large uncertainties characterize hazard forecasts involving induced activity. In addition, industrial activity is rapidly changing, and the sources of potentially induced earthquakes may change over the course of the next year.

Classification of Induced and Natural Earthquakes

Earthquake swarms, sequences of several earthquakes in a short period of time, are not unusual. We know that swarms of natural earthquakes can occur across the United States (such as the one near Sheldon, Nevada, that started in mid-2014), but nonetheless, it is widely accepted in the scientific community that swarms of induced earthquakes in the CEUS are quantitatively related to injection activities as measured by pumping volumes and rates (Ellsworth, 2013; McGarr and others, 2015; Weingarten and others, 2015). For this assessment, we classified earthquakes as induced or natural so that we could account for differences in earthquake source, frequency, propagation, and ground shaking

characteristics. Induced and natural earthquakes are thought to differ in several ways, and further research is needed to determine how they differ, but enough research is available to forecast such events. For example, observations worldwide of induced earthquakes indicate that their maximum magnitudes may be smaller than those for natural earthquakes, but many scientists also suggest induced earthquakes can trigger larger earthquakes on known or unknown faults (McGarr, 2014; Petersen and others, 2015a, b). Also, induced earthquakes tend to exhibit more swarmlike behavior and shallower average depths of rupture than many natural earthquakes (Gomberg and Wolf, 1999; Seeber and others, 2004; McNamara and others, 2015a; Skoumal and others, 2015a, b). Several models and observations suggest that induced swarms may have more small earthquakes compared to the numbers of large earthquakes (greater b-value; Benz and others, 2015; Petersen and others, 2015b). Hough (2014) suggested that high intensities close to the induced earthquakes are consistent with shallow depths, and low intensities at regional distances are consistent with low stress drop. Further, Atkinson (2015) compared empirical data from induced and natural earthquakes (NGA-West2 model) and determined that induced events may cause higher ground shaking close to the earthquake, possibly because of their shallow depths. Douglas and others (2013), however, indicated that ground shaking data from geothermally induced and natural earthquakes cannot be statistically distinguished; rather, they suggest that the ground motion distributions for natural and induced earthquakes may have different standard deviations. These discordant conclusions indicate that additional research is needed to better understand these differences.

We relied on published scientific research (table 1) and on consultations with State geological surveys and local experts (see Acknowledgements) to differentiate between induced and natural earthquakes (Davis and Frohlich, 1993). The scientific literature typically categorizes induced earthquakes by using one or more of the following criteria: (1) a statistically significant rate change of earthquakes (Llenos and Michael, 2013); (2) earthquakes located within a few kilometers of, and synchronous with, an active injection well and at depths consistent with injection (table 1); and (3) injection continuing or recently ceased at the time of the earthquake (table 1). The evidence for the activity being induced is especially compelling when reductions in the earthquake rate correlate with reductions in wastewater injection (McNamara and others, 2015b). For those earthquakes where origins remain unresolved, we considered alternative models to accommodate this uncertainty.

To classify induced and natural earthquakes for this assessment, we used polygonal shapes (in map view) to define 21 zones of induced seismicity that are thought to encompass areas of induced earthquakes occurring within a prescribed time interval (fig. 1, table 1). Any earthquakes located outside of these 21 zones are considered to be natural earthquakes for this informed model. The time interval corresponds to the period when anomalously high earthquake rates were observed or to periods of industrial activity as defined in the scientific literature. We also weighted each zone according to the support among the scientific community for its classification as induced; most zones were weighted using published studies, but we allowed for alternative customized weights for five zones to account for comments from State geological surveys and local experts. The weights applied to each zone and the bases for those weights are as follows: (1) 100 percent weight on induced branch—based on scientific literature and discussions with local experts who are in support of the classification (16 zones), (2) 80 percent weight on induced branch—based on scientific literature and discussions with local experts who are mostly supportive of this classification but wish to acknowledge alternatives (Raton Basin and North-central Arkansas), (3) 50 percent weight on induced branch—based on discussions with local experts supported by evidence of notable naturally occurring earthquakes (Brewton, Ala., and Sun City, Kans.), and (4) 0 percent weight on induced branch—based on expert opinion and little or no published science indicating that earthquakes are induced (Irving, Tex.).

We recognize that within some of these zones are earthquakes that occurred before the recent spate of wastewater injection activities, and it is possible that natural earthquakes are ongoing and interspersed with the induced events. For example, from 1950 to 2005, Oklahoma recorded an average of 1.5 earthquakes with a magnitude (M) greater than 3.0 per year, though some of these earlier earthquakes may also have been induced (Hough and Page, 2015). Over the past few years, however, Oklahoma has recorded several hundred M3.0+ earthquakes per year, many of which are thought to be related to wastewater injection. Nevertheless, there is no reason to believe that the background rate of natural earthquakes has decreased during this recent flurry of activity. Other regions such as central Arkansas and the Raton Basin, Colo. and N. Mex., are also thought to experience both induced and natural earthquakes. We are likely including a few natural (tectonic) earthquakes in our zones of induced seismicity, but as observed in Oklahoma, the numbers of natural earthquakes within these zones are probably quite low compared to numbers of induced earthquakes, so we do not account for this complication in the current assessment.

Seismic Hazard Models Including Induced and Natural Earthquakes in the CEUS

In this paper, we forecast the CEUS ground shaking hazard by including contributions from both natural and induced earthquakes. We used earthquake information collected through the end of 2015 to assess the hazard for a 1-year period—the forecast expires at the end of 2016.

We used two models to account for earthquake classification as induced or natural: the informed model considers the possibility that induced earthquakes differ from natural earthquakes, and the adaptive model does not differentiate between the two types of earthquakes. We also considered alternative earthquake source and ground motion models by using a logic-tree (or decision-tree) framework, in which weights were applied to each parameter based on the degree of acceptance in the scientific community regarding which is best for forecasting earthquakes and associated ground shaking.

Methodology

The seismic source and ground motion models we used are the most important components of this analysis; for details on faults and other parts of the hazard model, refer to the 2014 NSHM documentation (Petersen and others, 2014, 2015a, b). The seismicity rate model assumes that patterns and rates of smaller earthquakes (M2.7–4.7) can be used along with a truncated Gutenberg-Richter magnitude-frequency distribution (Gutenberg and Richter, 1944) from the minimum considered magnitude to the maximum magnitude (Mmax) to forecast the rates and locations of large earthquakes (Frankel, 1995; Petersen and others, 2014). In this analysis, we incorporated catalogs with shorter duration than were applied in the 2014 NSHM because we are only forecasting earthquake rates for 2016. The ground motion models are primarily based on limited ground shaking recordings of global earthquakes in stable continental regions as well as ground shaking simulations using earthquake source and crustal properties consistent with this region. This is an active area of research to better define the differences between induced and natural earthquake ground shaking.

We used two logic trees for this assessment, one for sites located within zones of reported induced seismicity and another for sites located outside of these zones (fig. 3). We include both alternative logic trees because we want to be able to treat earthquakes within zones of induced seismicity differently from other earthquakes. We need both sets of logic trees to produce a seismic hazard map that includes influences from earthquakes within and outside of the zones. These components were combined to forecast the rates and locations of earthquakes across the CEUS.

Differences between the logic trees are primarily found in the parameters of the seismicity model (labeled "rate model" on fig. 3), which involves the catalog duration, smoothing distance, and maximum magnitude, and those of the ground motion model. Figure 3*A* shows the logic tree for sources within zones of induced seismicity, and figure 3*B* shows the logic tree for sources outside the zones.

A

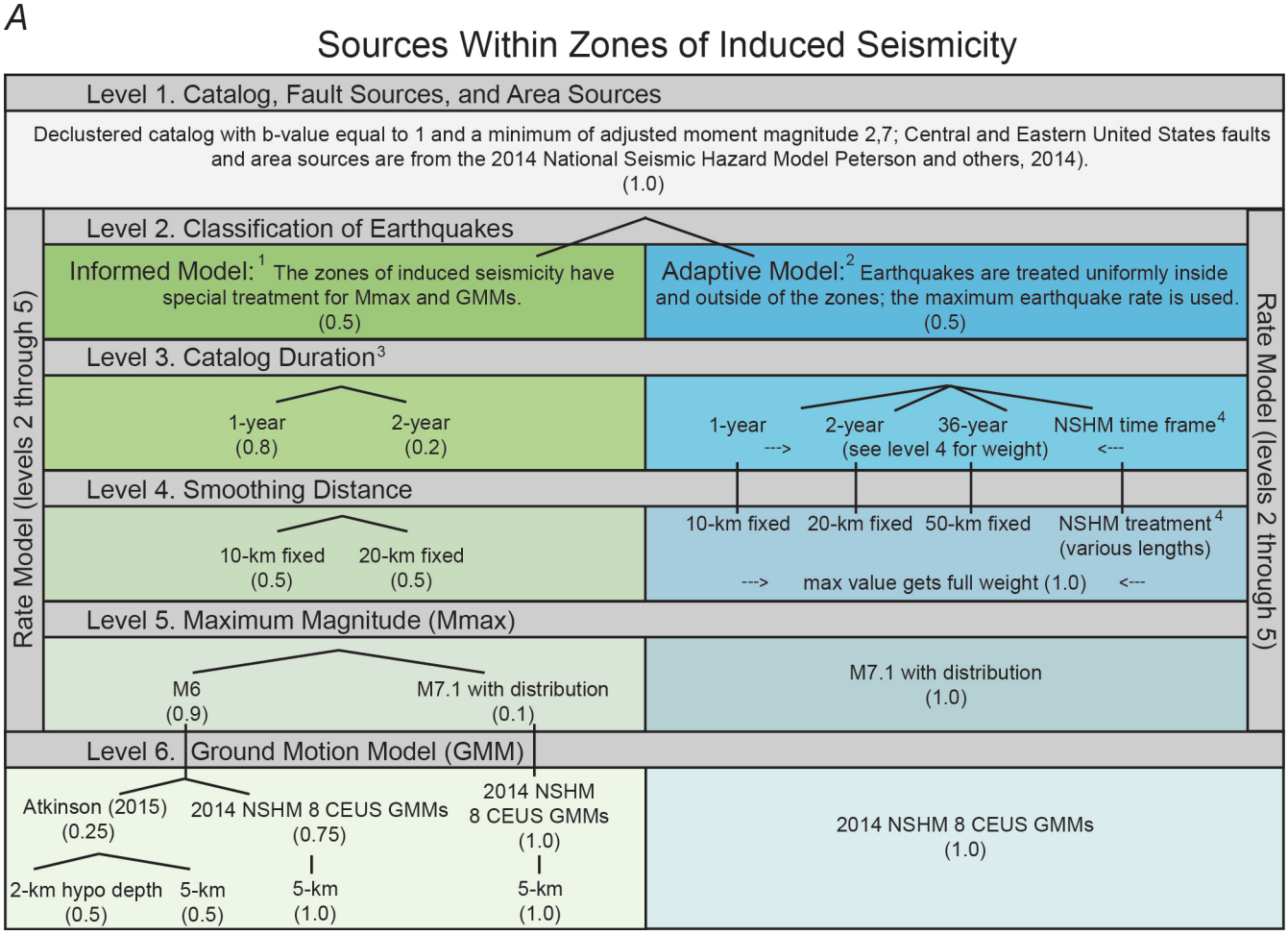

Figure 3. Two logic trees applied in the 2016 one-year seismic hazard model. *A*, For sites within defined zones of induced seismicity. *B*, For sites outside of zones of induced seismicity. (NSHM, National Seismic Hazard Model; km, kilometer; M, moment magnitude; Mmax, maximum magnitude; GMM, ground motion model; hypo, hypocentral; CEUS, Central and Eastern United States. See table 1 and figure 1 for details on the zones of induced seismicity used in this assessment.)

[1] In the informed model, unresolved zones are given special weight to acknowledge that (1) at this time, there is no scientific consensus regarding the classification of earthquakes as potentially induced, as with Brewton, Irving, and Sun City, or (2) the zone is in a tectonically active area with some natural earthquakes, as with the North-central Arkansas and Raton Basin zones. These decisions were made with input from State geologists and local experts. Weights for these zones are shown in table 1, column 2.

[2] See appendix 2 for more information on the adaptive model.

[3] In the informed model, for sites inside the zones but outside of the corresponding time windows shown in table 1, column 7, the seismic hazard is equivalent to the 2014 NSHM. The informed model in figure 3*B* shows how the values are derived. [This footnote applies to figure 3*A* only.]

[4] The long-term model will have similar treatment as the 2014 NSHM (Petersen and others, 2014) for the adaptive model, but a key difference for the informed model is that the catalog will now include earthquakes from 2013 through 2015.

B

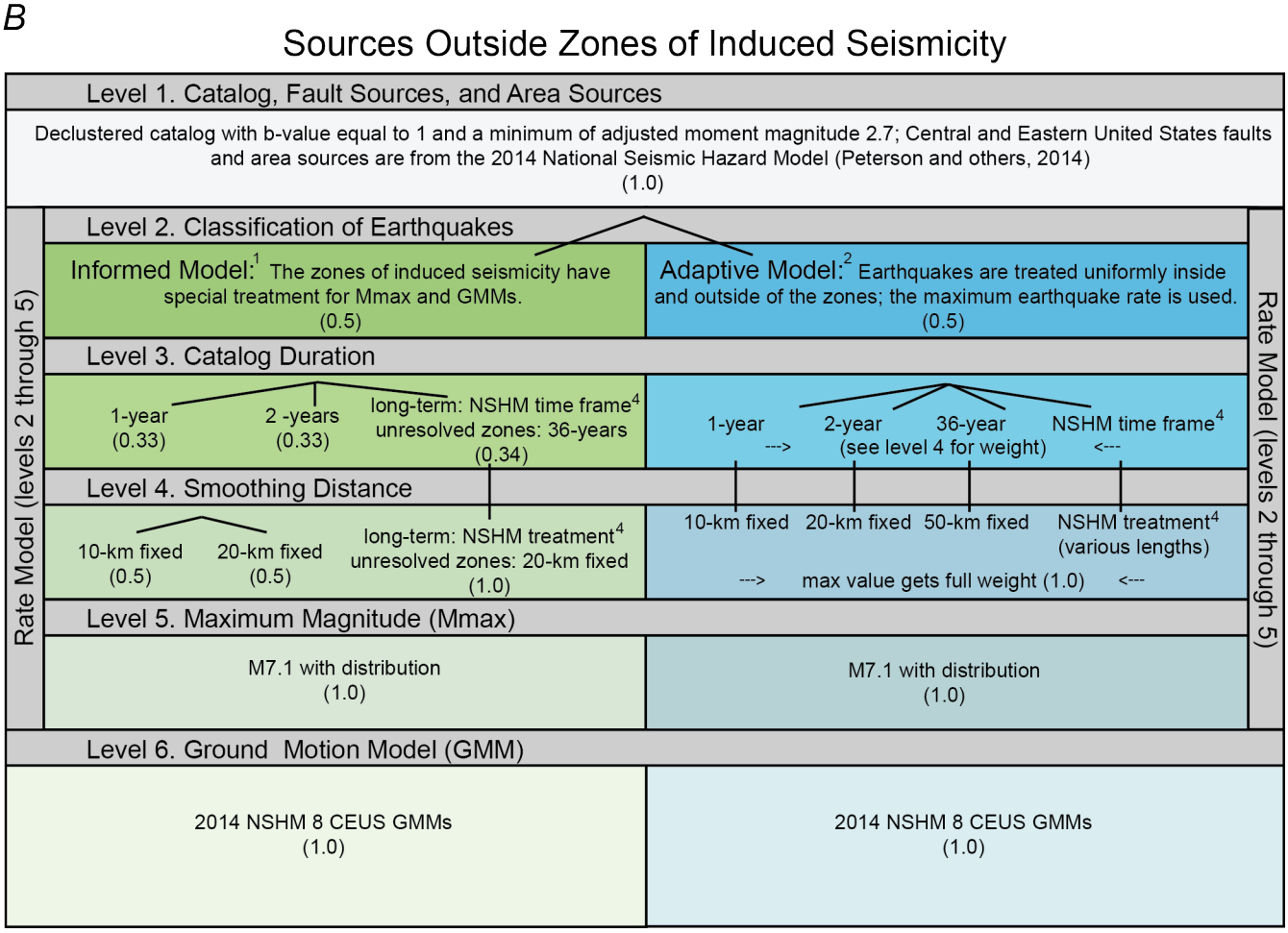

Figure 3. Two logic trees applied in the 2016 one-year seismic hazard model. *A*, For sites within defined zones of induced seismicity. *B*, For sites outside of zones of induced seismicity. (NSHM, National Seismic Hazard Model; km, kilometer; M, moment magnitude; Mmax, maximum magnitude; GMM, ground motion model; hypo, hypocentral; CEUS, Central and Eastern United States. See table 1 and figure 1 for details on the zones of induced seismicity used in this assessment.)—Continued

[1] In the informed model, unresolved zones are given special weight to acknowledge that (1) at this time, there is no scientific consensus regarding the classification of earthquakes as potentially induced, as with Brewton, Irving, and Sun City, or (2) the zone is in a tectonically active area with some natural earthquakes, as with the North-central Arkansas and Raton Basin zones. These decisions were made with input from State geologists and local experts. Weights for these zones are shown in table 1, column 2.

[2] See appendix 2 for more information on the adaptive model.

[3] In the informed model, for sites inside the zones but outside of the corresponding time windows shown in table 1, column 7, the seismic hazard is equivalent to the 2014 NSHM. The informed model in figure 3*B* shows how the values are derived. [This footnote applies to figure 3*A* only.]

[4] The long-term model will have similar treatment as the 2014 NSHM (Petersen and others, 2014) for the adaptive model, but a key difference for the informed model is that the catalog will now include earthquakes from 2013 through 2015.

Model Development: Logic Tree for Sources Within Induced Zones (Figure 3*A*)

This section describes the levels of figure 3*A*, the logic tree for sites within induced zones, in detail. Level 1 describes an earthquake catalog that extends to the end of 2015 and fault and area sources from the 2014 NSHM (Petersen and others, 2014, 2015a). Level 2 describes the classification of earthquakes as induced or natural and the estimation of earthquake rates. Level 3 describes the durations of the earthquake catalogs that best predict earthquakes. Level 4 describes the smoothing parameters applied in the model. Level 5 describes the maximum magnitudes applied in the model. Level 6 describes the alternative ground motion models.

Level 1: Catalog and Earthquake Sources

Level 1 of the logic tree describes the catalog, fault sources, and area sources. This level is the same for both logic trees, that is, for sites both within and outside of zones of induced seismicity (fig. 3*A*, *B*); we did not allow for alternatives at this level. For this assessment, we produced a declustered catalog (Gardner and Knopoff, 1974) with a minimum magnitude of M2.7. The declustered catalog for induced seismicity is consistent with a b-value of 1.0 and a catalog completeness level of M2.7 since about 1980 (Petersen and others, 2015b). Tests show that a larger b-value may be appropriate if the full, non-declustered catalog is applied in the analysis. We tested the sensitivity of hazard when applying other catalogs with other minimum magnitude thresholds, without declustering, and with varying b-values and determined that the catalogs and parameters we have chosen provide a reasonable estimate of earthquake rates with sufficient detail for this application (Petersen and others, 2015b). We decided to apply the declustered catalog in this model for the following reasons: (1) the probabilistic method as defined by Cornell (1968) requires a catalog with independent earthquakes, (2) the 2014 NSHM and previous versions all applied declustered catalogs, and (3) it allows us to compare hazard in the CEUS with other places across the United States (for example, California). Because the CEUS induced seismicity sequences are swarmlike, the Gardner and Knopoff (1974) declustering methodology may underestimate the hazard. In some cases, such as following the 2011 Prague, Okla., earthquake, this declustering methodology may remove some independent earthquakes. It is important to point out that if we were to apply the full catalog rather than a declustered catalog, the hazard may be significantly higher than what we show in this model (Petersen and others, 2015b). Assessing the best methods for declustering the catalog or determining if the full catalog should be included in the hazard assessment will help to determine the hazard.

Level 2: Alternative Models for Classifying Induced and Natural Earthquakes

The second level considers two alternative models to classify earthquakes in the CEUS: (1) the informed model, which assumes that earthquakes can be broadly classified as induced or natural based on scientific information and literature, and (2) the adaptive model, which assumes that we cannot distinguish between induced and natural earthquakes (appendix 2). The informed model treats induced and natural earthquakes differently, allowing for the application of recent research on induced earthquakes. This model also allows for earthquake rate decay. The adaptive model uses a uniform approach across the CEUS and does not distinguish between induced and natural earthquakes. It does not depend on judgments about areas and time windows of induced seismicity. The adaptive model does not allow for a short-term decay of earthquake rates because it uses the maximum earthquake rate determined from alternative catalog time windows. Both informed and adaptive models are useful for this analysis and we have weighted them equally.

Level 3: Earthquake Catalog Duration

The third level defines the catalog durations used to forecast earthquake rates: 1-year (2015), 2-year (2014–2015), or 36-year (1980–2015) durations or the long-term duration applied in the 2014 NSHM (1700–2012) extending through 2015 for the informed model (fig. 2). It is important to note that the 2014 NSHM and its long-term catalog consider variable completeness levels across the CEUS (Petersen and others, 2014), but this study uses a uniform CEUS-wide completeness threshold of M2.7 for the 1-year, 2-year, and 36-year catalogs.

There are several reasons for considering varying catalog lengths: (1) it is likely that earthquakes that occurred during the most recent time will best predict the next year's activity; (2) sometimes the induced seismicity goes through alternating periods of heightened activity and dormancy that are not predictable without other industry information on fluid injection and extraction; and (3) sometimes, though injection has stopped, earthquakes can occur months or years later in the vicinity of the injection well (such as the Rocky Mountain Arsenal zone; Evans, 1966; Healy and others, 1968). Though all four catalog durations used in this assessment provide important earthquake rate information, the informed and adaptive models use different durations and assign them different weights (compare the "Catalog Duration" level in fig. 3*A* to the same level in fig. 3*B*).

Informed Model

For calculating the hazard for an earthquake source within a zone, the informed model for induced earthquakes assumes that a 1-year catalog is the most effective predictor of the earthquake rate for the following year. We gave this catalog the most weight because statistical studies indicate that the shorter time window is better than longer periods of earthquake observations in predicting the next year's rate (appendix 1). Nevertheless, we also allowed for a catalog that uses a 2-year duration, but we gave it less weight. This emphasis on short-term catalog durations was suggested by local experts who attended our workshop. In addition to being better for forecasting earthquake rates for the following year, application of short-term durations have the added benefit that hazard is reduced in places where earthquake rates are decreasing in response to regulation of wastewater disposal or for other reasons.

To calculate the informed model hazard for sources inside of induced zones, we applied a seismicity rate floor based on the 2014 NSHM (Petersen and others, 2014; fig. 3 footnotes). As discussed, we considered 21 zones as potentially encompassing induced seismicity. A total of 12 zones had activity during the 2-year catalog, and of those, 8 zones had potentially induced seismicity during the 1-year catalog. The remaining 9 zones, which were inactive during the past two years, are modeled with the 2014 NSHM hazard inputs. Additionally, 5 of the 21 zones were considered with partial weight (see section "Classification of Induced and Natural Earthquakes").

Adaptive Model

For the adaptive model, catalog durations were applied the same way for earthquake sources inside and outside of the zones. This model considers the maximum earthquake rate from among the 1-year, 2-year, 36-year, and 2014 NSHM catalogs to assess the hazard (appendix 2). This alternative model accounts for hazard in areas that may be experiencing an increase in seismicity over a longer time scale.

Level 4: Smoothing Distances Applied in Predictive Model

The fourth level involves the smoothing distance applied in calculating the gridded rates (Frankel, 1995). Earthquakes above M2.7 are counted in each grid cell, the Gutenberg-Richter model is

applied to get rates (10^a), and the rates are then smoothed spatially using a Gaussian operator. This branch is constrained by a series of likelihood tests to determine the optimal smoothing distance needed to forecast earthquakes (appendix 1). Level 4 of figure 3*A* outlines the smoothing distances that correspond to the four catalog durations used in level 3. Results of the statistical study for induced earthquakes indicate that shorter smoothing distances and recent, short-term catalogs provide better forecasts than larger smoothing distances and longer catalogs. These smoothing distances are also more compatible with the distances observed between induced earthquakes and the causative deep disposal wells. Because we are making a 1-year hazard forecast instead of a longer 50-year forecast, and because we are able to utilize recent earthquakes that are more accurately located, scientists at our workshop felt that we should use a smaller smoothing distance than the 50-kilometer (km) to 75-km smoothing kernel applied in the 2014 NSHM to avoid over-smoothing the hazard. For sources inside the zones, the informed model allows for Gaussian smoothing kernels of 10-km and 20-km fixed widths, and the adaptive model allows for a broad range of distances including 10-km, 20-km, 50-km, and 2014 NSHM widths (Petersen and others, 2014).

Level 5: Maximum Magnitude (Mmax)

The fifth level considers a maximum magnitude (Mmax) for the largest size of earthquake that can occur in the region. The Mmax we applied for natural earthquakes is the same as that applied in the 2014 model, with a mean of M7.1 and a broad distribution (Petersen and others, 2014). The Mmax distribution is based on earthquake sizes observed in similar tectonic regions across the globe (Petersen and others, 2014). For the informed model, we consider an Mmax of M6 or a distribution with a mean of M7.1 for induced earthquakes. Many of the participants at our workshops felt that the lower Mmax branch should receive the most weight for sites within zones because we have not observed earthquakes greater than M6 that were thought to be caused by wastewater injection. For the adaptive model, we only consider the 2014 NSHM Mmax model.

Level 6: Ground Motion Models

The sixth level involves the ground motion models. In addition to the set of ground motion models used for computing CEUS hazard for the NSHM (Petersen and others, 2014), we also considered a model developed by Atkinson (2015) for the informed model. This Atkinson (2015) model was compared to induced earthquakes in Canada and is thought to represent a reasonable alternative for induced earthquake shaking. Nevertheless, this model was developed using NGA-West2 ground motion models (for example, from data derived from the Western United States and other active tectonic regions) instead of data from the stable continental regions, so the model was down-weighted compared to the 2014 NSHM ground motion models applied for the CEUS region (fig. 3*A*). Earthquake depth is an important factor in calculating ground shaking. According to McNamara and others (2015a, b), most induced earthquakes in Oklahoma occur in bedrock with depths around 5 km. Consistent with the 2014 NSHM, we used a 5-km depth for the eight CEUS ground motion models for calculating distance from the rupture source (there is no depth-dependent ground motion term in any of these CEUS ground motion models). For the Atkinson (2015) model, we applied 2-km and 5-km hypocentral depth alternatives in our analysis because these changes make differences in areas very close to the earthquake source and we cannot rule out shallower depths. The induced ground motion model of Atkinson was only considered for the informed model for sites within the zones and was only applied for $M \leq 6$ earthquakes; the model is applied within 100 km of an earthquake hypocenter, unlike the suite of eight CEUS ground motion models that are applied out to 1,000 km in the 2014 NSHM. For the adaptive

model, we only applied the suite of CEUS ground motion models that were applied in the 2014 NSHM (Petersen and others, 2014).

Model Development: Logic Tree for Sources Outside of Induced Zones (Figure 3*B*)

The logic tree for sources outside of induced zones is shown in figure 3*B*. Levels 1 and 2 are identical for sources located within and outside of the induced zones. The adaptive model also is the same for sources located inside and outside of the zones. This discussion, therefore, only pertains to how the informed model for sources outside of the zones (fig. 3*B*) differs from the informed model for sources within the zones (fig. 3*A*).

For Level 3, "Catalog Durations," additional catalogs were considered. To calculate the informed model hazard for sources outside of induced zones, we considered 1-year and 2-year catalogs and the long-term catalog applied in the 2014 NSHM (1700–2012) extending through 2015 for the informed model. Also, we used the 36-year catalog in lieu of the long-term catalog for the unresolved zones (shown in red in figure 1*A* and table 1). In this way, the potentially induced earthquakes that are several decades old will be excluded from the model. Jordan and Jones (2010) indicated that short-term models demonstrate a probability gain in forecasting earthquakes relative to the long-term, time-independent models typically used in seismic hazard analysis. Therefore, for these short-term hazard assessments, we applied equal weighting to the various catalog durations.

For Level 4, "Smoothing Distance," we applied 10-km and 20-km smoothing distances for the 1- and 2-year catalogs (appendix 1) and the 50- to 75-km smoothing options from the 2014 NSHM (Petersen and others, 2014). Smoothing distances for the branch that applies to the NSHM long-term catalogs are the same as in the 2014 NSHM (Petersen and others, 2014). The unresolved zones (shown in red in figure 1*A* and table 1) were modeled using the 20-km smoothing for the 36-year catalog.

For levels 5 and 6, we only applied the M7.1 Mmax with distribution option and the suite of CEUS ground motion models that were applied in the 2014 NSHM (Petersen and others, 2014).

Results

We developed 1-year seismic hazard maps, hazard curves, and Modified Mercalli Intensity (MMI) maps to illustrate the 2016 hazard forecast for the CEUS. Each of these different products portrays seismic hazard information useful for understanding potential ground shaking and earthquake effects. In this section, we show the hazard for the alternative branches used in this assessment to illustrate the broad uncertainties therein.

Seismic Hazard Maps

We have produced seismic hazard maps based on 1-percent probability of exceedance in 1 year for the year 2016 that include induced and natural earthquakes (generally consistent with an annual 1/100 probability or rate of exceedance). We calculate the 1-percent probability of exceedance in 1 year hazard because (1) we only want to forecast one year of seismicity, (2) we want to consider relatively small chances of shaking in 1 year, and (3) these probability levels were suggested at our workshop. The maps are generated for peak horizontal ground acceleration (PGA) and spectral acceleration at 1-hertz (Hz; 1-second) and 5-Hz (0.2-second) frequencies. They are made for a uniform site condition with a Vs30 (shear-wave velocity in the upper 30 meters) of 760 meters per second—although some of the intensity maps are modified for site condition. We calculate the hazard at a grid of sites separated by about 0.1 degree latitude and longitude across the United States.

Some of the input parameters contribute more to the overall hazard uncertainty than other parameters. We produced PGA comparison maps to illustrate the sensitivity of the ground shaking when selecting the 1-year or 2-year catalogs, the 10-km or 20-km Gaussian smoothing parameters, the M6 or M7.1 Mmax, and the Atkinson (2015) ground motion model with 2-km or 5-km depths or the CEUS suite of ground motion models. (The Atkinson [2015] model only applies for M6 earthquakes and smaller.) This sensitivity study shows the basic elements of an uncertainty analysis. For the purpose of this comparison, we assume a base case defined by the 1-year catalog, 10-km smoothing applied to the Gaussian kernel, an M7.1 Mmax, and the CEUS suite of ground motion models. Figure 4 shows difference and ratio comparisons for PGA between alternative catalog durations (fig. 4*A*), smoothing distances (fig. 4*B*), Mmax (fig. 4*C*), and ground motion models (fig. 4*D*).

A

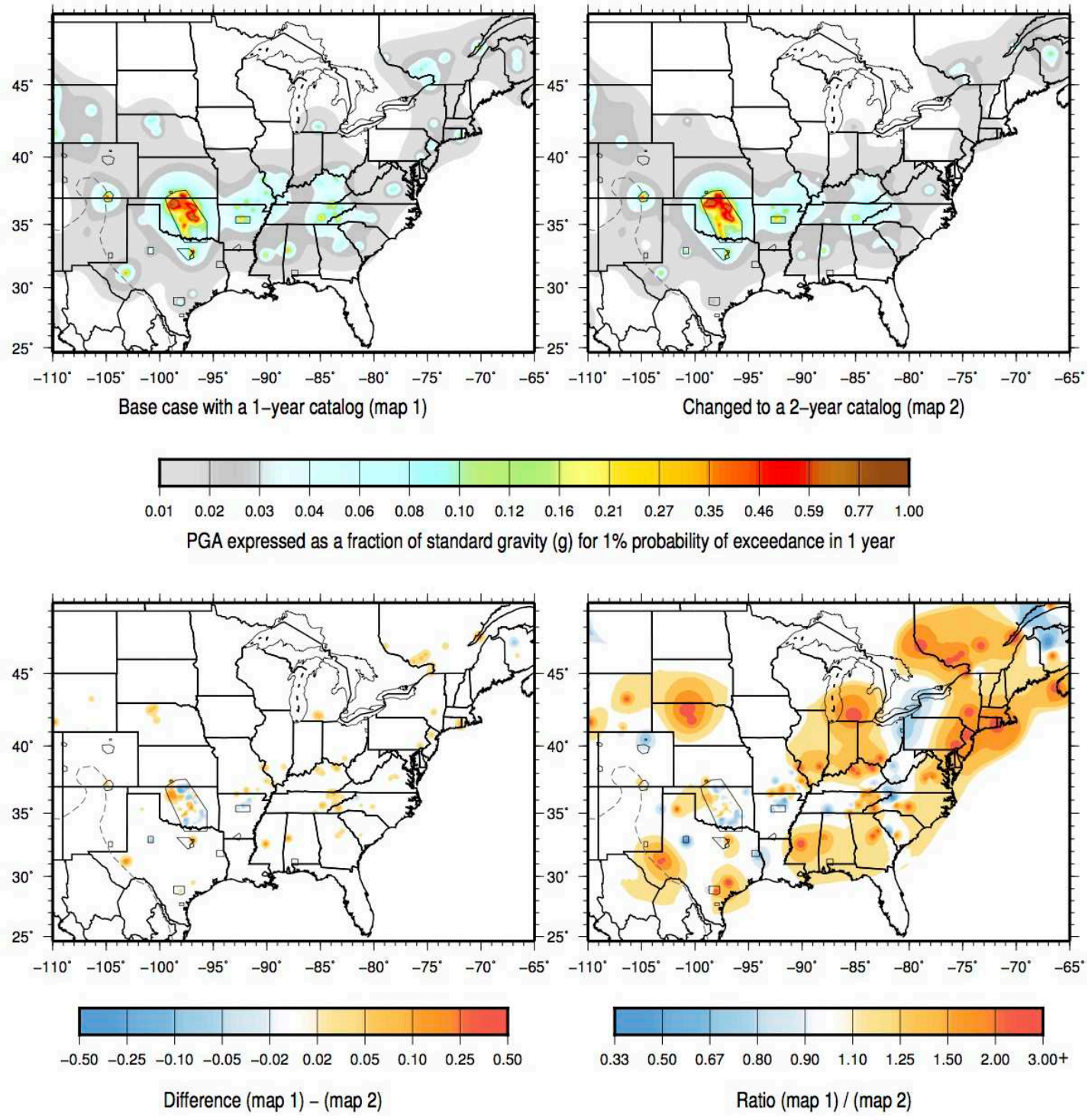

Figure caption on page 26.

B

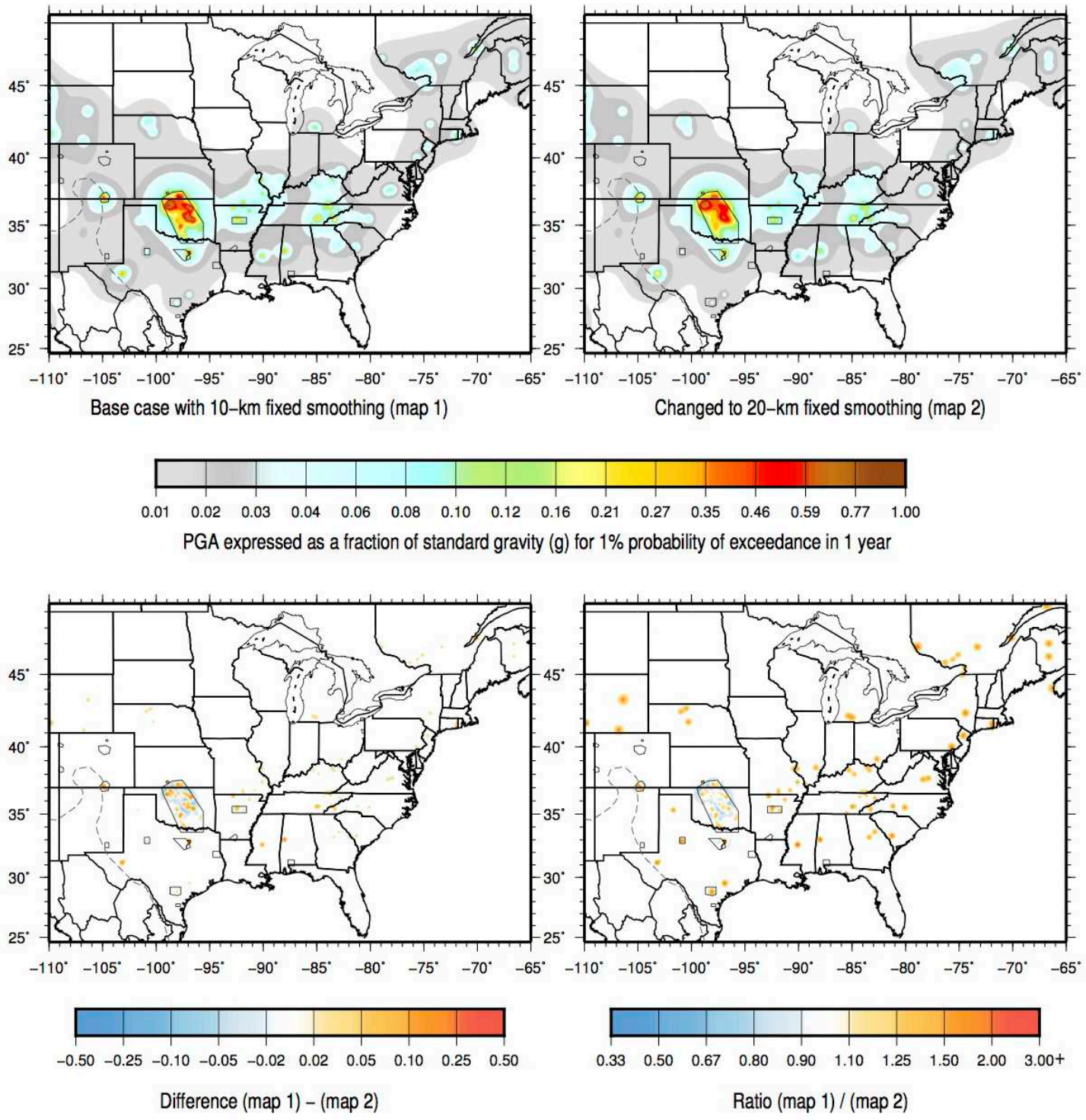

Figure caption on page 26.

C

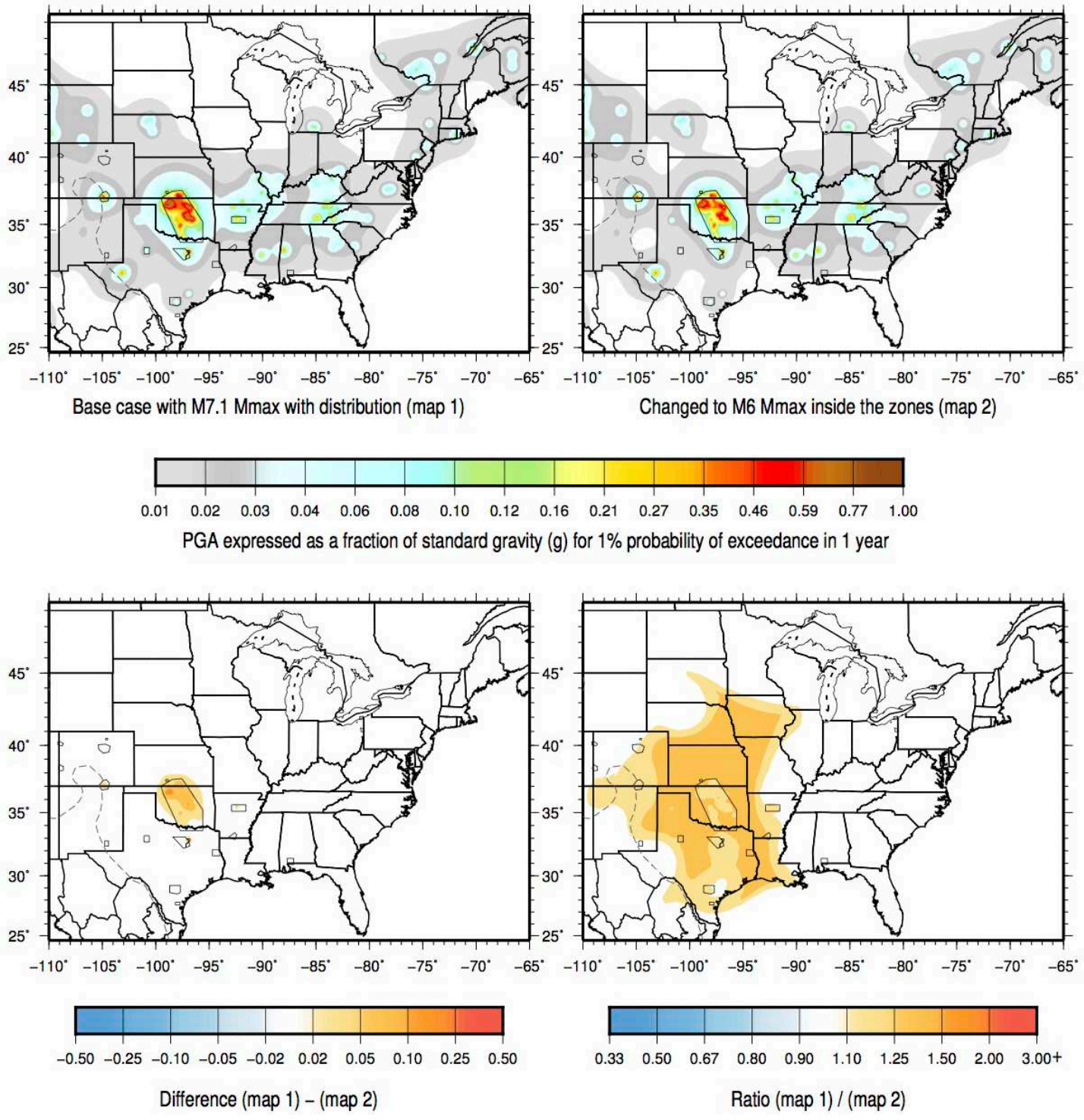

Figure caption on page 26.

D

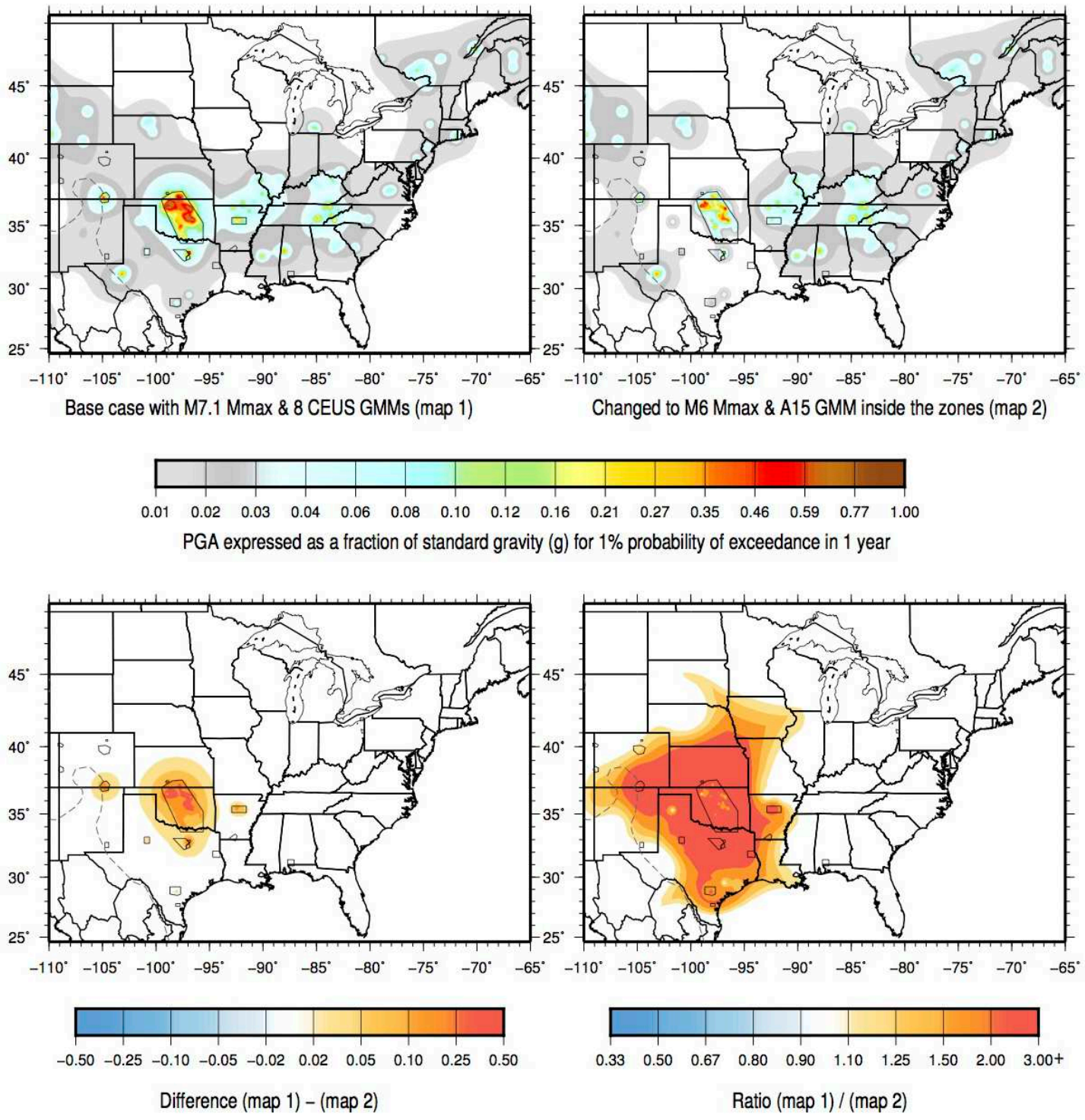

Figure caption on page 26.

Figure 4. Peak horizontal ground acceleration hazard maps showing sensitivity to input parameters relative to a base case (the base case, shown in the upper left, is the same for all parts of the figure). For *A*–*D*, the difference (lower left) is the base case (upper left) minus the model with the varied parameter (upper right), and the ratio (lower right) is the base case divided by the model with the varied parameter. Gray dashed line indicates western boundary of the Central and Eastern United States (CEUS). *A*, Sensitivity for catalog duration. Base map: 1-year catalog. Varied parameter: includes a 2-year catalog. *B*, Sensitivity for smoothing distances. Base map: 10-kilometer (km) smoothing parameter. Varied parameter: incorporates a 20-km smoothing parameter. *C*, Sensitivity for maximum magnitude (Mmax). Base map: moment magnitude (M) 7.1 Mmax. Varied parameter: M6.0 Mmax (within zones). *D*, Sensitivity for ground motion model (GMM). Base map: M7.1 Mmax and CEUS GMM. Varied parameters: incorporates an M6 Mmax—the equation does not apply for earthquakes above M6—and incorporates the Atkinson (2015) GMM for 2-km rupture depth.

Figure 4*A* shows the PGA ground motions from the 1-year and 2-year catalogs. The differences, which are generally within ±0.05 g with ratios mostly between 10 and 50 percent, reflect the variability in the earthquake locations between the two catalogs.

Figure 4*B* shows the PGA hazard changes caused by varying the smoothing distances (10 and 20 km). Changes to the hazard are mostly within ±0.02 g but in localized areas can be up to ±0.05 g. This is consistent with ratios of about ±25 percent. Hazard is more centrally focused with the smaller kernel.

Figure 4*C* shows the PGA hazard changes at sites within the zones caused by varying the Mmax. (There are no Mmax differences outside of the zones.) The Mmax used in the 2014 NSHM causes increased ground motion up to 0.1 g in northern Oklahoma and ratio increases up to 50 percent in the seismic hazard over a broad area, compared to the model which applies the lower M6.0 Mmax. This result seems reasonable because the mean Mmax of M7.1 used in the 2014 NSHM allows for earthquakes larger than an Mmax of M6.0. The increases are even greater for the 1-Hz (1-s) spectral acceleration ground motions when applying the 2014 model. This result shows that it is important for the science community to better understand the sizes of induced and natural earthquakes. This Mmax parameter may be better defined by examining faults at or beneath the surface and applying scaling relationships between moment magnitude and fault length or area (McNamara and others, 2015b).

Figure 4*D* shows the PGA hazard changes caused by varying the ground motion model and Mmax. The reason we change these simultaneously is because we cannot calculate ground shaking using the Atkinson (2015) model for M≥6 earthquakes and we do not use this ground motion model outside of the zones. For ground motions outside of the zones, we only apply the 2014 NSHM CEUS ground motion models and the 2014 Mmax distribution centered at M7.1. Therefore, the hazard changes for varying ground motion models are only applicable within the zones and are associated with the smaller Mmax of M6.0. The hazard changes are large and widespread when varying the models. The 2014 NSHM ground motion model causes increases of 0.25 g compared to the Atkinson (2015) model. The 2014 ratios show higher ground shaking levels (between a factor of 2 and 3) over a broad area of Oklahoma, Kansas, Colorado, New Mexico, Texas, Missouri, and Arkansas compared to ground motions from the Atkinson (2015) model. Directly over the areas of very active seismicity in Oklahoma, ground motions are only about 10–25 percent higher. This comparison also seems reasonable because the Atkinson (2015) model indicates particularly high ground motions near the earthquake but fall off faster than typical CEUS models—because it is based on models for the Western United States. This result also points out the importance of improving our understanding of ground motion from induced and natural earthquakes.

Figure 5 shows comparisons of the adaptive and informed models (fig. 5*A*) and the final models for PGA (fig. 5*B*), as well as comparisons of 1-Hz (1-s; fig. 5*C*) and 5-Hz (0.2-s; fig. 5*D*) spectral accelerations obtained by equally weighting the adaptive and informed models. The differences between the informed and adaptive models show the effect of characterizing induced and natural earthquakes. The final model plots show our best estimate for three ground motion frequencies. These final maps are compared with the 2014 NSHM to show the changes in hazard due to the inclusion of induced earthquakes and earthquake rate changes.

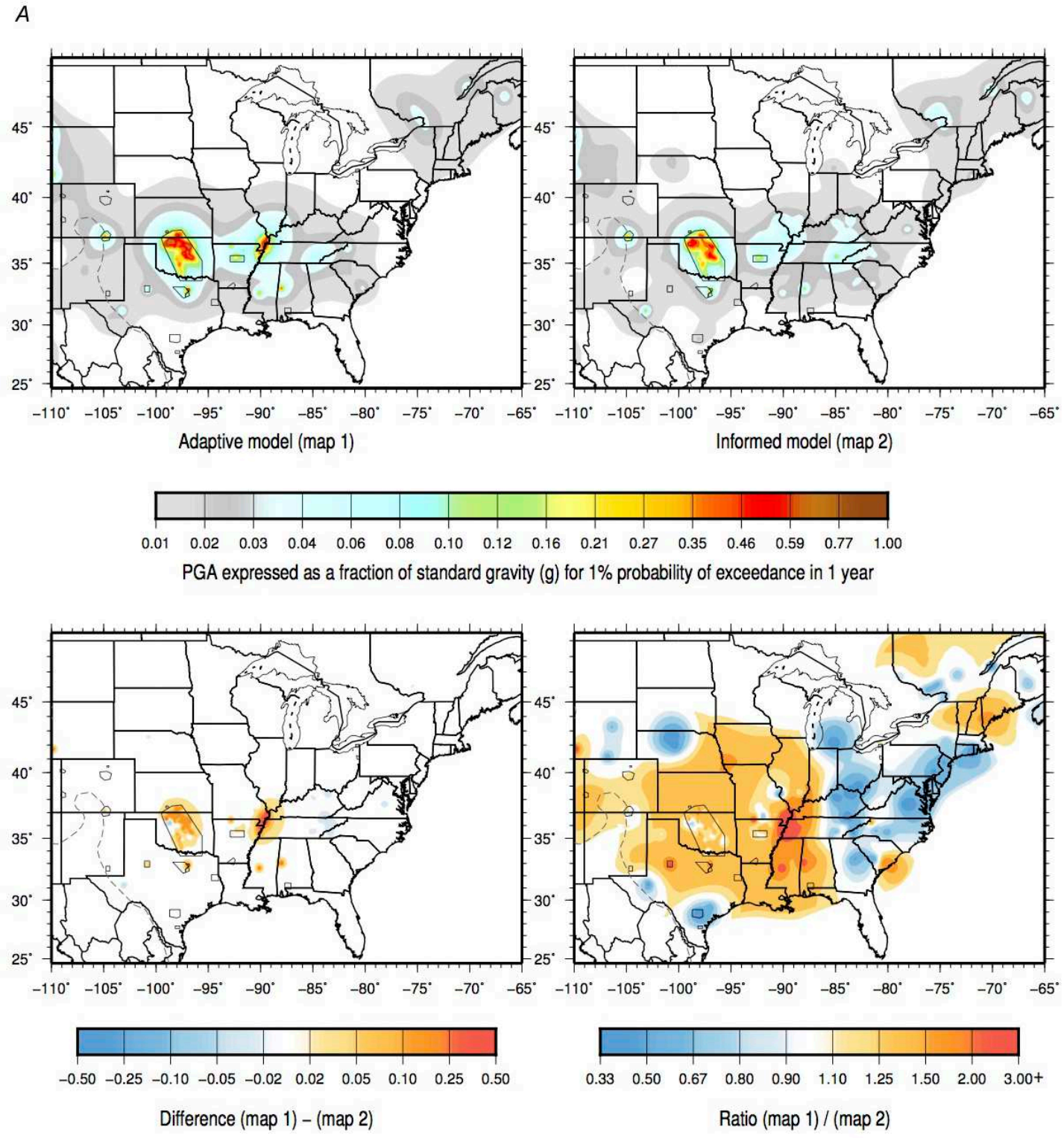

Figure caption on page 32.

B

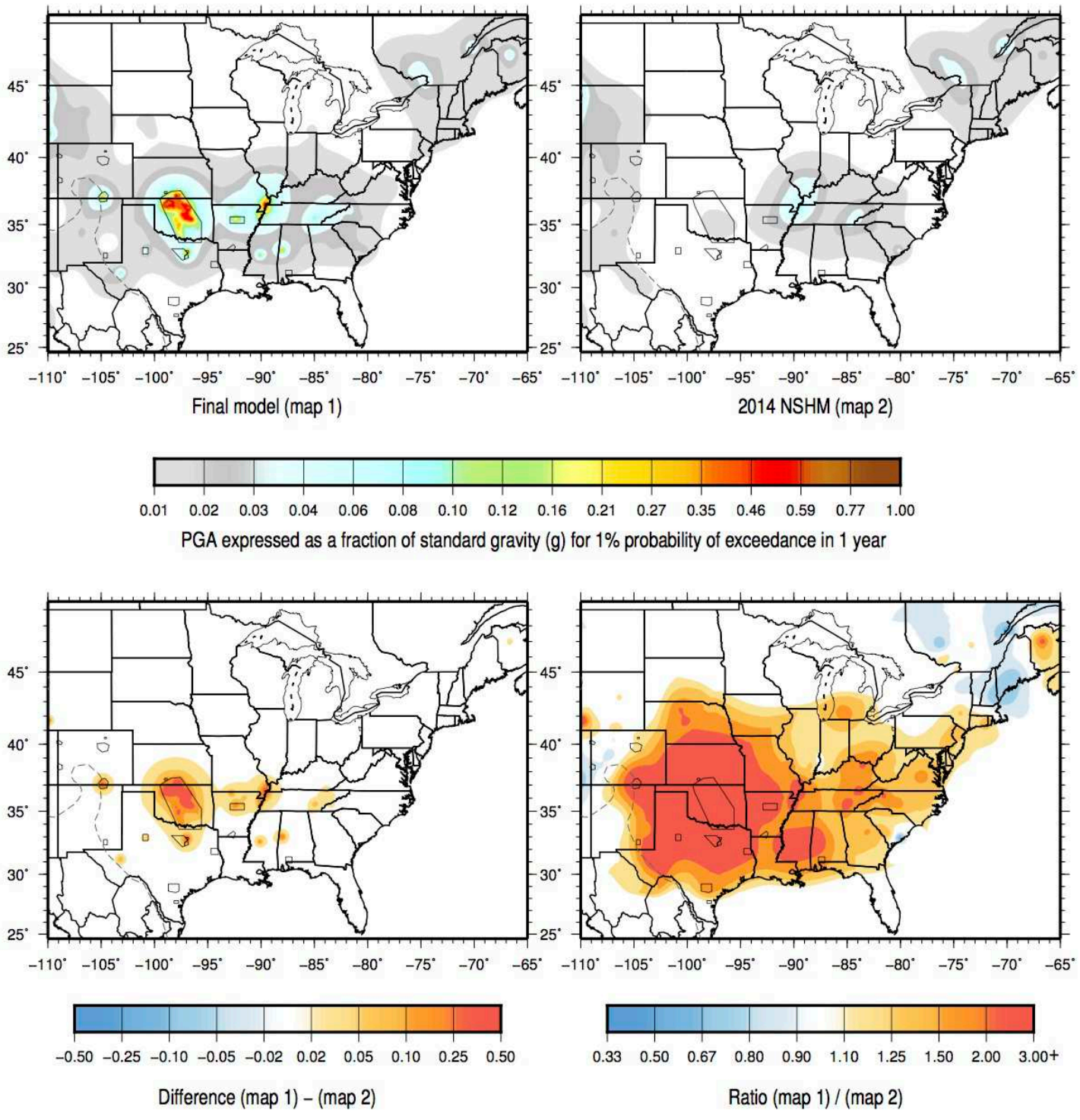

Figure caption on page 32.

C

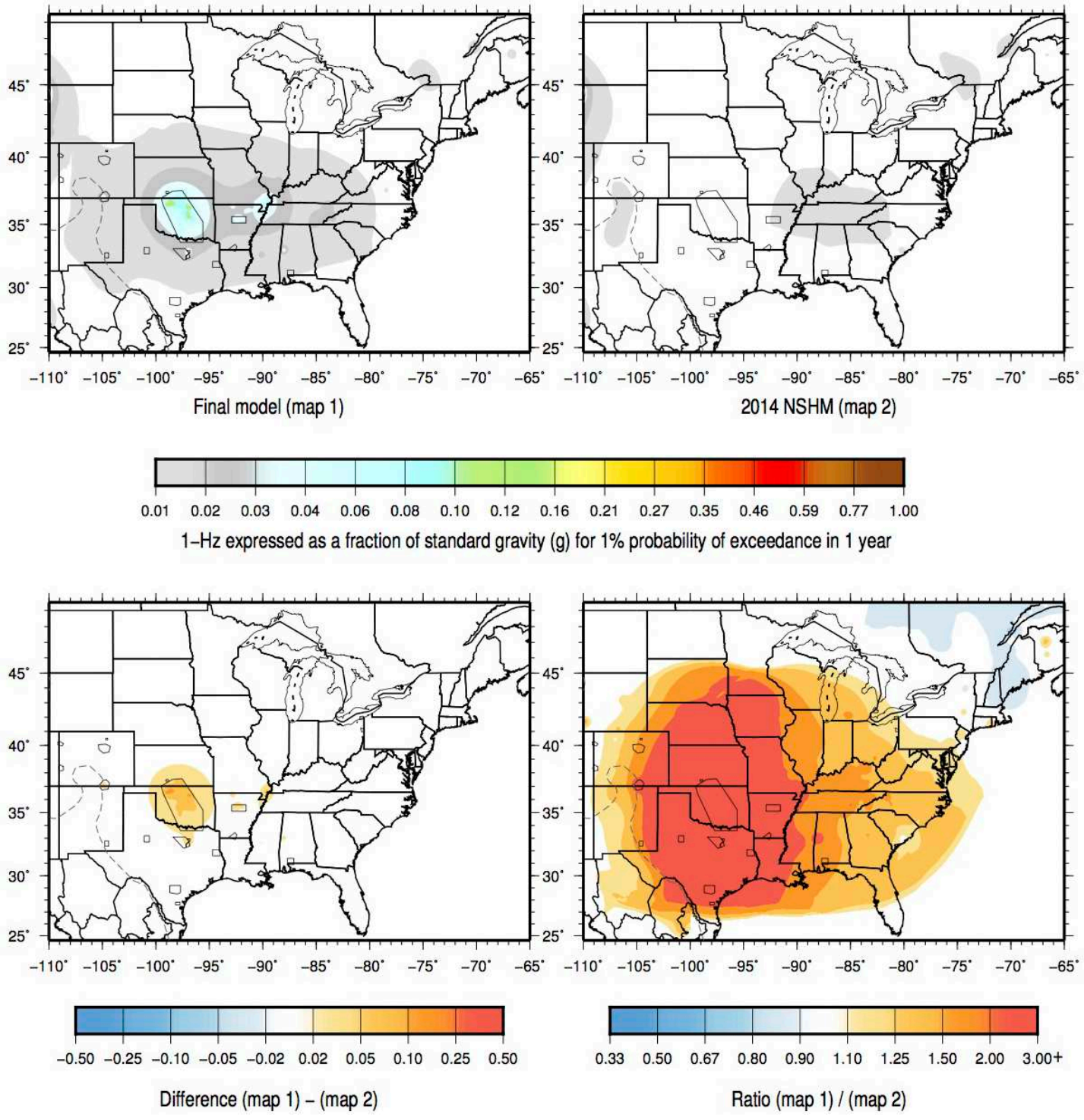

Figure caption on page 32.

D

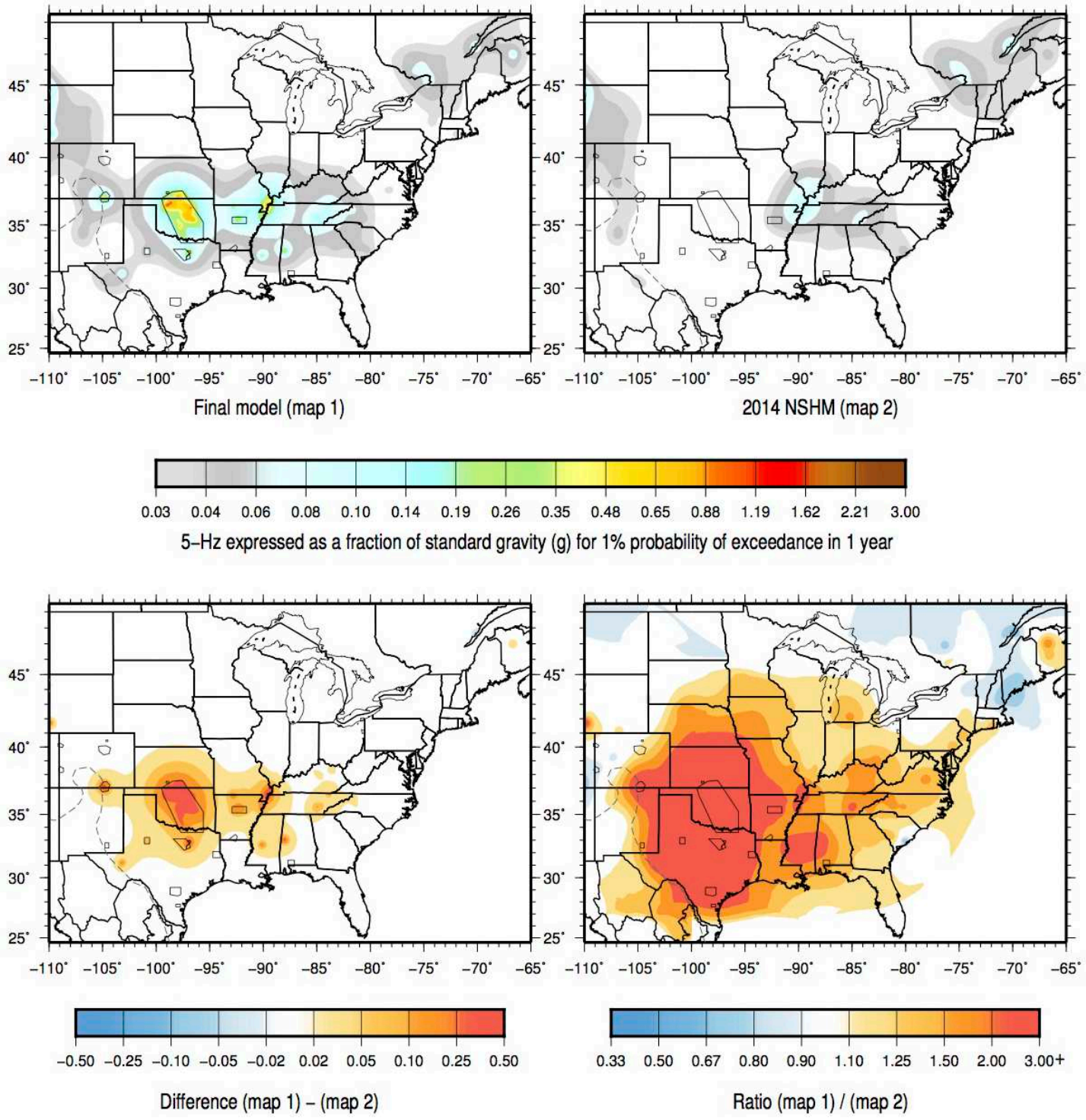

Figure caption on page 32.

Figure 5. Comparisons of the hazard maps 1-percent probability of exceedance in 1 year for adaptive and informed models and for the final model and the 2014 National Seismic Hazed Model (NSHM). For *A–D*, the difference (lower left) is the upper left map minus the upper right map, and the ratio (lower right) is the upper left map divided by the upper right map. Gray dashed line indicates western boundary of the Central and Eastern United States (CEUS). The New Madrid Seismic Zone, referenced in the text, is located in southeastern Missouri, northeastern Arkansas, and adjacent parts of Tennessee and Kentucky. *A*, Peak horizontal ground acceleration (PGA) ground motion hazard: upper left shows hazard based on the adaptive model, upper right shows hazard based on the informed model. *B*, PGA hazard: upper left shows the final hazard for the 2016 one-year model, upper right shows the hazard for the 2014 NSHM. *C*, 1-hertz (Hz; 1-second) spectral acceleration hazard: upper left shows the final hazard for the 2016 one-year model, upper right shows the hazard for the 2014 NSHM. *D*, 5-hz (0.2-second) spectral acceleration hazard: upper left shows the final hazard for the 2016 one-year model, upper right shows the hazard for the 2014 NSHM.

Figure 5*A* shows the PGA hazard for the adaptive and informed models. The adaptive model is generally similar to the informed model within zones of induced seismicity. In general, in places where the adaptive model hazard is higher than the hazard from the informed model, the difference is caused by the methodology of selecting the maximum earthquake rate. Alternatively, in places where the informed model hazard is higher than the adaptive model hazard, the difference is caused by the trimming of earthquakes applied in the adaptive model (appendix 2). Nevertheless, both models (adaptive and informed) produce large hazard in active zones of induced seismicity, despite fundamental differences in how the earthquakes are classified (natural or induced). The ground motion ratio between the adaptive and informed models is ±50-percent for most of the CEUS; the difference is up to 0.25 g. The hazard at the New Madrid Seismic Zone (southeastern Missouri, northeastern Arkansas, and adjacent parts of Tennessee and Kentucky) is higher in the adaptive model than the informed model because of the following differences: (1) earthquake rates from short-term 1-year and 2-year catalogs are higher than rates from long-term catalogs, (2) the adaptive model uses the maximum earthquake rates from alternative catalog durations, (3) the informed model uses earthquake rates from the 2014 NSHM long-term catalog for New Madrid, and (4) the adaptive model applies only the 10-km smoothing distance for the 1-year catalog, which increases rates over the earthquake locations (fig. 3).

Figure 5*B* shows the PGA hazard for the final 2016 one-year model, which weights the adaptive and informed models equally. We compare the final model to the 2014 model that does not consider induced earthquakes. The 2016 seismic hazard is higher by more than a factor of 3 almost everywhere in the CEUS compared to the 2014 model, mostly because of increases in the potentially induced seismicity throughout the CEUS over the past decade. The ±50-percent ratios between the adaptive and informed models are smaller in most areas compared to ratios between the 2016 one-year model and the 2014 NSHM, which are more than a factor of 3 in areas of induced activity.

Hazard Curves

Hazard curves show ground motion levels on the x-axis and annual frequency of exceedance on the y-axis. Figure 6 shows hazard curves for several populated places near induced earthquakes: Oklahoma City and Waynoka, Okla.; Anthony, Kans.; Greenbrier, Ark.; Dallas, Tex.; and Trinidad, Colo. The highest curves, for the Oklahoma and Kansas sites, are due to high rates of induced earthquakes over the past decade. Curves for Greenbrier and Trinidad are lower than the Oklahoma curves by about a factor of 2 or more. The Dallas curve shows more variability in shape because it is influenced by the distant Oklahoma seismicity but is very close to the north Texas activity. Most of the 2016 hazard curves are higher than the 2014 model in these locations by an order of magnitude.

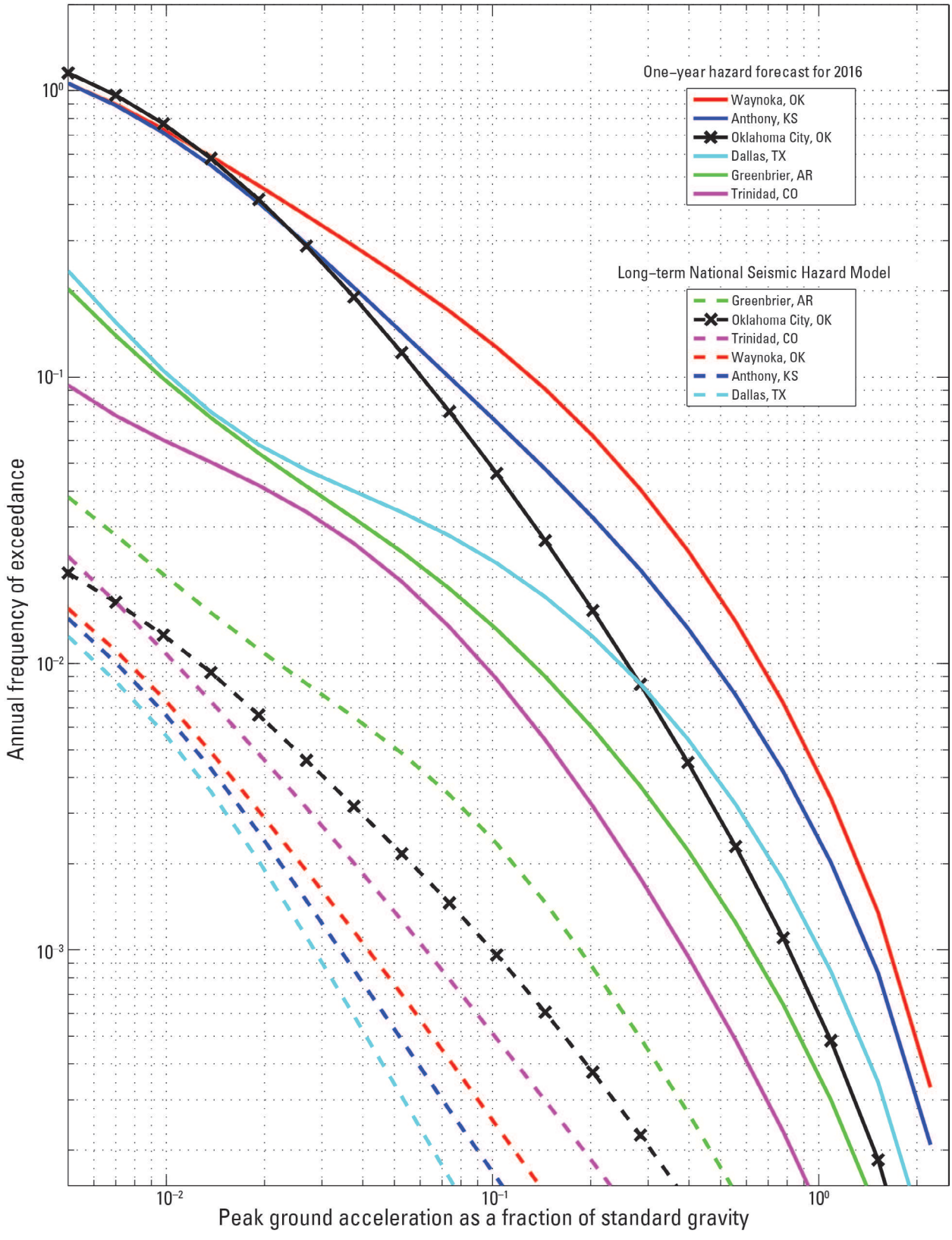

Figure 6. Peak horizontal ground acceleration hazard curves for towns and cities located near induced earthquakes for the 2016 one-year model and for the 2014 National Seismic Hazard Model.

Modified Mercalli Intensity Maps

Many users prefer models that portray earthquake shaking intensity (MMI) or earthquake effects (see, for example, the USGS ShakeMap products, http://earthquake.usgs.gov/earthquakes/shakemap) rather than more quantitative measures of ground shaking presented in our previously described hazard maps. The MMI scale uses Roman numerals, typically ranging from I to X, to describe how people feel the earthquake and how much damage occurs at a site. For example, shaking at intensities of MMI I, II, or III is generally light and either not felt or felt very weakly. Intensities of MMI IV and V are felt by many, but the earthquake shaking typically causes only limited damage to windows or dishes. An intensity of MMI VI indicates minor damage such as fallen plaster or cracks in the walls, and intensities of MMI VII, VIII, IX, and X are related to heavier damage. For the purposes of this forecast, we use MMI VI as the threshold of damage.

Figures 7*A* and 7*B* show MMI maps for the United States that include the 2014 NSHM for the Western United States and the 2016 one-year model for the CEUS (the 2014 NSHM is a long-term model displayed for 1-percent chance of exceedance in 1 year, and the 2016 model is a short-term model). We have included the 2014 NSHM long-term tectonic hazard in these plots so that we can compare it with CEUS earthquake rates. We used the Wald and Allen (2007) topographic-based site classification to assess the soils at each grid point applied in the calculations. We applied the equations of Worden and others (2010) to translate the PGA and 1-Hz (1-s) spectral acceleration ground motions into MMI. The ground motions were then amplified based on the Stewart and Seyhan (2013) amplification factors. The maps using PGA to calculate MMI (fig. 7*A*) show quite high MMI (VIII or more) and larger areas of potential damage than the maps that apply 1-Hz (1-s) spectral acceleration (fig. 7*B*). The maps that use 1-Hz (1-s) spectral acceleration to obtain MMI (fig. 7*B*) only reach about MMI VI; they do not allow for the larger intensities observed during the 2011 Prague, Okla., earthquake (MMI VII–VIII; Hough, 2014). Nevertheless, the maps based on 1-Hz (1-s) spectral acceleration may give results that are more similar to peak velocities, which are often thought to be a better predictor of damage than other frequencies. Worden and others (2010) discussed combining various measures to obtain more robust MMI estimates, so we have averaged the PGA-based and 1-Hz (1-s) spectral acceleration-based MMI maps to obtain the final map for this report (see next section, “Final Maps”).

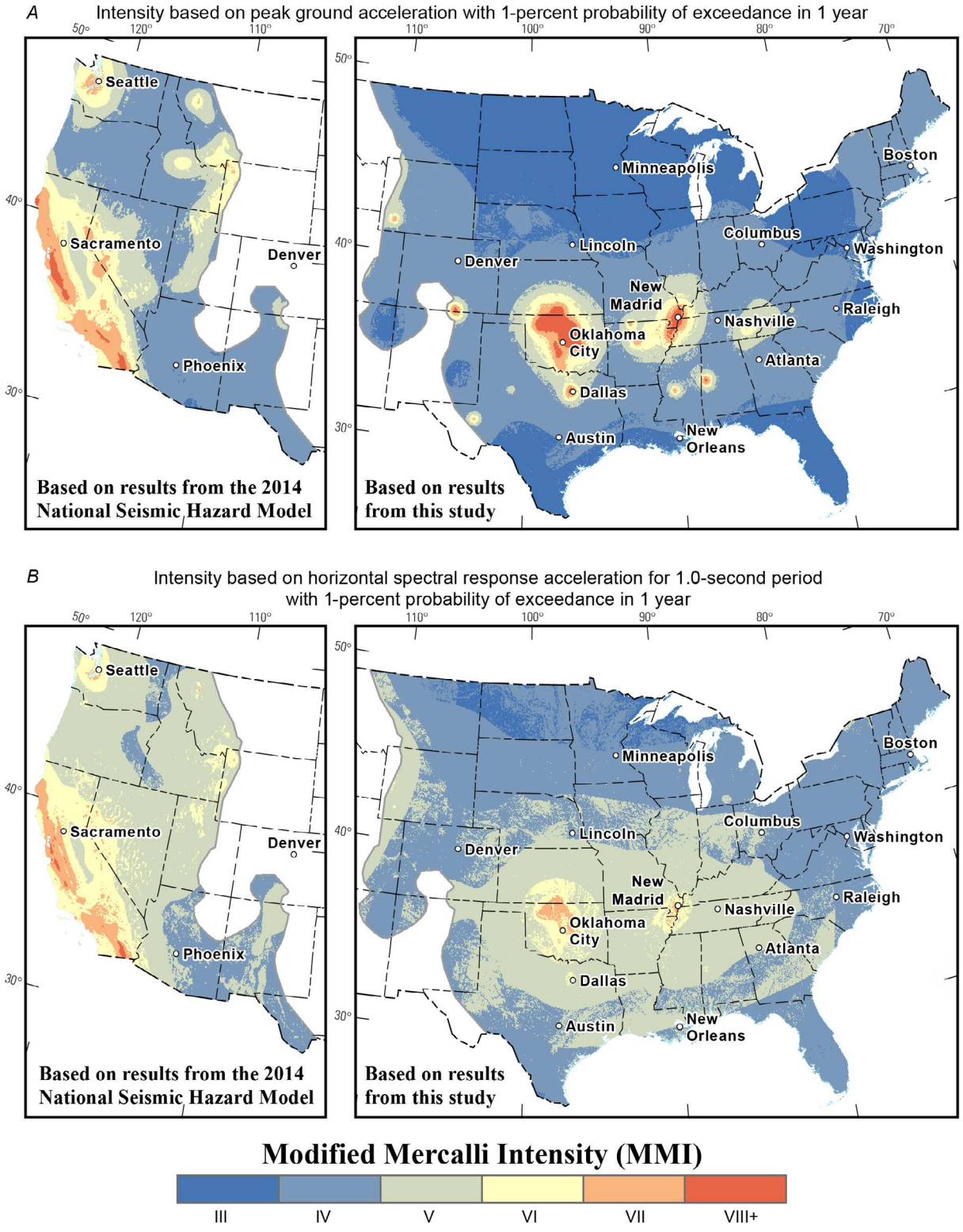

Figure caption on page 37.

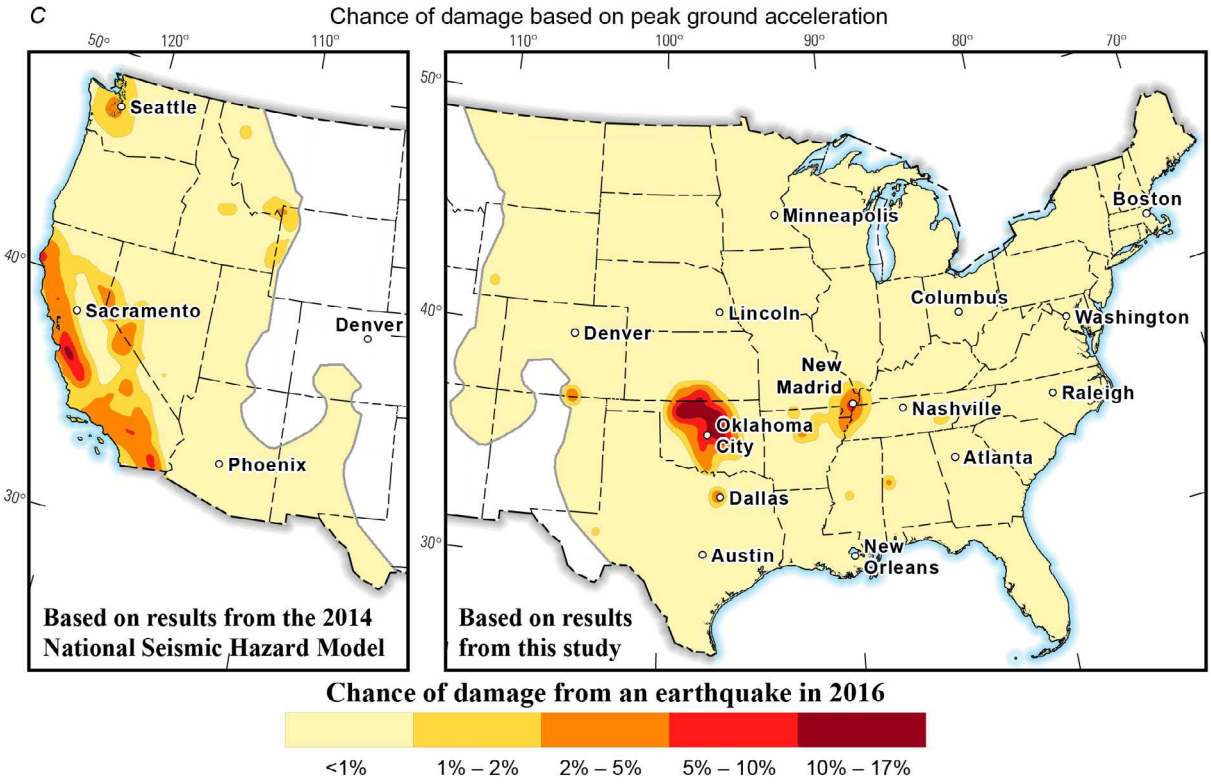

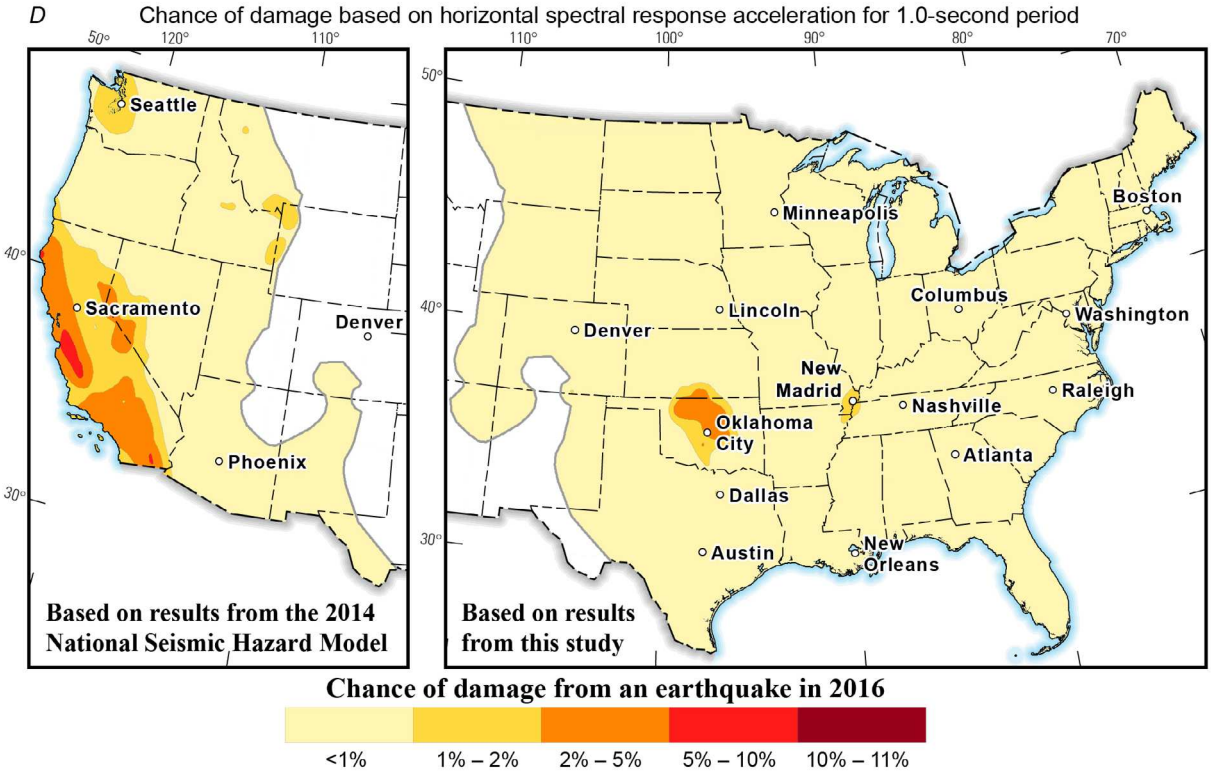

Figure caption on page 37.

Figure 7. Modified Mercalli Intensity maps and chance of damage for the Western United States and the Central and Eastern United States (CEUS) based on peak horizontal ground acceleration and 1-hertz spectral acceleration. For *A*–*D*, the map of the Western United States shows data based on the long-term 2014 National Seismic Hazard Model, and the map of the CEUS shows data based on the 2016 one-year model. *A*–*B*, Modified Mercalli Intensity (MMI) maps at 1-percent probability of exceedance in 1 year for the United States obtained (*A*) by converting peak horizontal ground acceleration (PGA) to MMI and (*B*) by converting 1-hertz (Hz; 1-second) spectral acceleration to MMI. These maps (*A* and *B*) are site amplified. *C*–*D*, Chance of damage (MMI greater than or equal to VI) from an earthquake in 2016, obtained from the rate of occurrence of (*C*) PGA ground motions and (*D*) 1-Hz (1-second) ground motions that are correlated with MMI VI for a uniform alluvial soil (National Earthquake Hazards Reduction Program site class D).

Figures 7*C* and 7*D* show maps of the United States that also include the 2014 NSHM long-term tectonic hazard for the Western United States for comparison with the 2016 model hazard for the CEUS. In these maps, we consider the chances of experiencing damaging earthquakes for a fixed ground shaking level that corresponds with MMI VI (0.12 g PGA and 0.10 g 1-Hz [1-s] spectral acceleration). As in figures 7*A* and 7*B*, figures 7*C* and 7*D* show higher hazard for the PGA-based MMI compared to MMI obtained from converting 1-Hz (1-s) spectral acceleration. A weighted combination (average) of these maps may provide a more robust estimate of the potential earthquake intensity (MMI).

Final Maps

The final hazard maps show forecasts for MMI values and the chance of damaging earthquakes (MMI of VI or more). These parameters may be more comprehensible for many people than unconverted PGA or spectral acceleration values (fig. 8). Figure 8A presents an MMI map with a 1-percent probability of exceedance in 1 year for the United States obtained by averaging figures 7A and 7B. Sites in north-central Oklahoma, southernmost Kansas, central Arkansas, the Dallas-Fort Worth area, and the Raton Basin near the border of Colorado and New Mexico show MMI values that are greater than VI, VII, or VIII. Forecasted ground shaking in the north-central Oklahoma and Dallas, Tex., regions are consistent with damage levels observed over the past decade (Wald and others, 2011).

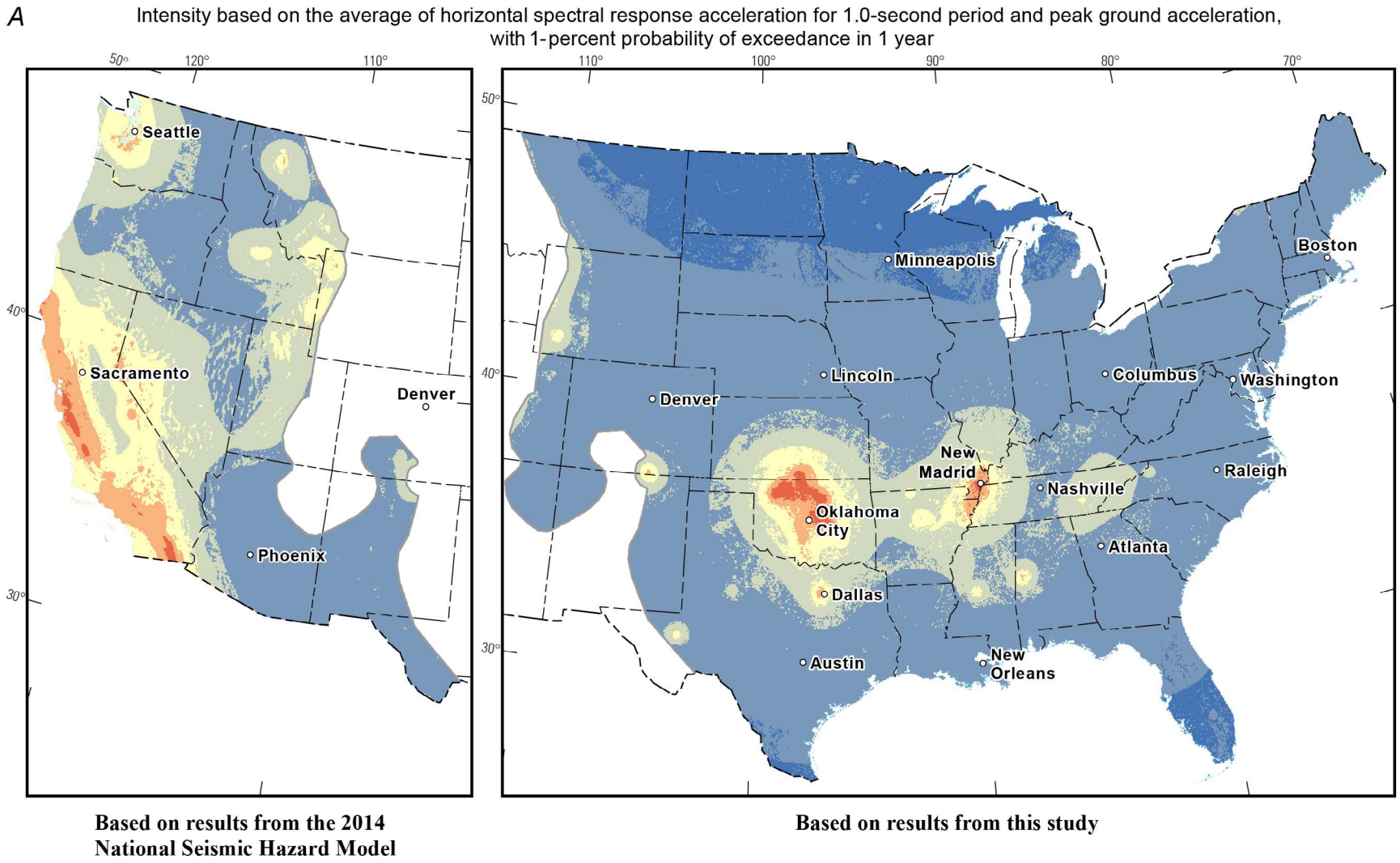

Figure caption on page 40.

B Chance of damage based on the average of horizontal spectral response acceleration for 1.0-second period and peak ground acceleration

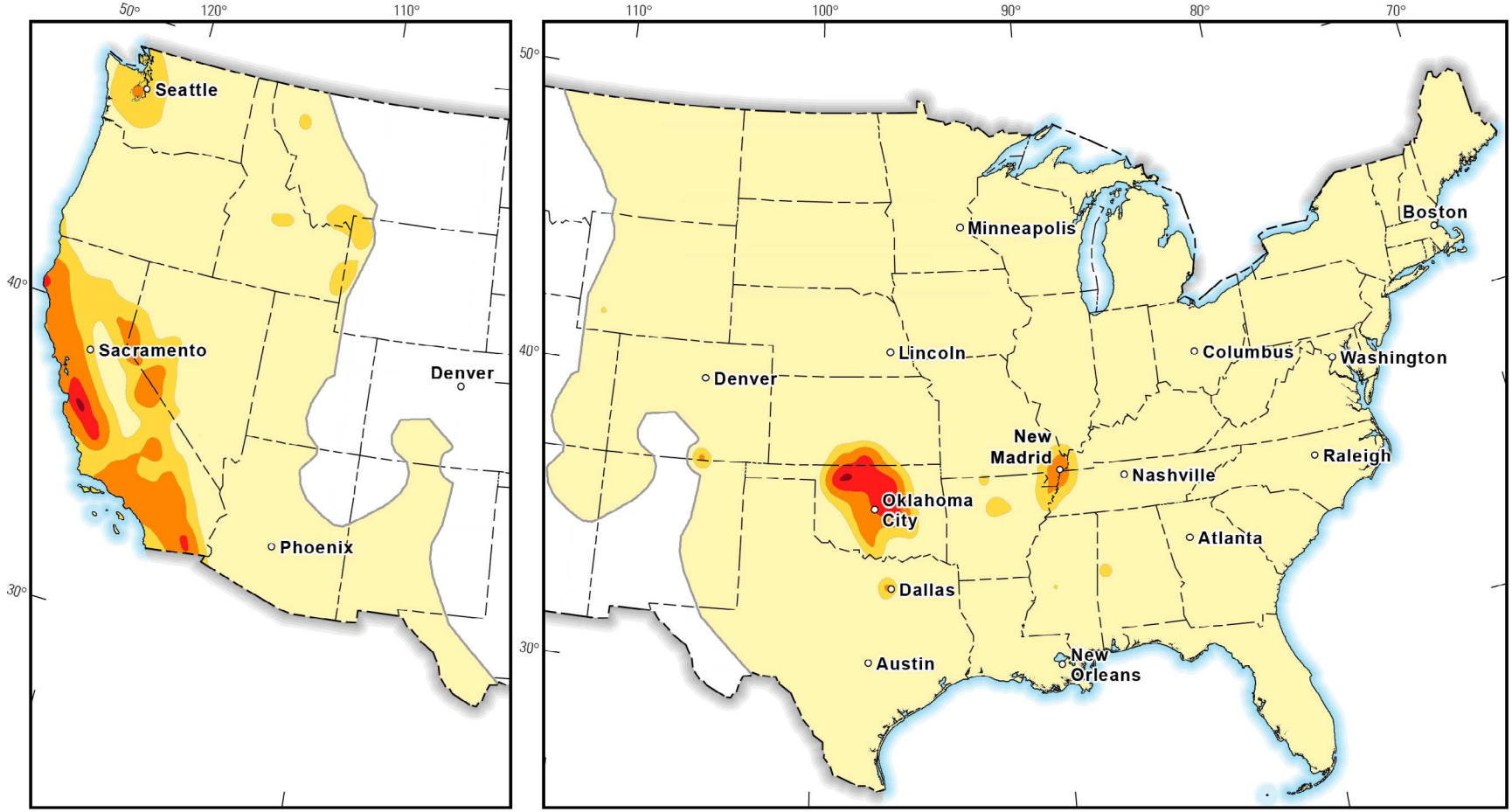

Figure caption on page 40.

Figure 8. Final hazard maps for Modified Mercalli Intensity (MMI) and chance of damage for the Western United States and the Central and Eastern United States (CEUS) based on averages of MMIs converted from peak horizontal ground acceleration and 1-hertz spectral acceleration. For *A*–*B*, the map of the Western United States shows data based on the long-term 2014 National Seismic Hazard Model, and the map of the CEUS shows data based on the 2016 one-year model. *A*, Modified Mercalli Intensity (MMI) map at 1-percent probability of exceedance in 1 year for the United States obtained by averaging figures 7*A* and 7*B*. *B*, Chance of damage from an earthquake during 2016 obtained by averaging figures 7*C* and 7*D*.

Many of the places where damage is likely in our 2016 model have experienced damage in the past decade. The USGS operates a "Did You Feel It?" Web tool to archive and analyze responses from individuals who have felt an earthquake. These responses are then assigned a shaking intensity (Wald and others, 2011). Since 2010, responses from earthquakes have been associated with MMI VI or greater in states experiencing induced earthquakes. About 1,500 individual citizen reports greater than MMI VI have been archived by "Did You Feel It?": 1,300 in Oklahoma, 102 in Kansas, 50 in Arkansas, 42 in Texas, and 6 in Colorado and New Mexico (V. Quitoriano and D. Wald, USGS, written commun., 2016). This information, however, includes responses for all earthquakes, so it is possible that some of these events (especially from eastern Arkansas) may not correspond with induced earthquake activity. Nevertheless, the recent induced activity in these states is probably creating many or most of the responses collected with the "Did You Feel It?" tool.

The second version of the map (fig. 8*B*) shows the chance of damage from an earthquake during 2016 using the same results as applied in figure 8*A*. The chance of having an event with MMI VI or greater is over 10 percent per year in north-central Oklahoma and southernmost Kansas. This chance of damage in parts of Oklahoma is similar to the chance of damage at high-hazard sites in California. More research is needed, however, to better quantify how recorded ground motions relate to observed damage from induced earthquakes. Figure 8*B* shows the chance of damage from an earthquake in 2016 by averaging the exceedance probabilities obtained from PGA at 0.12 g and 1-Hz (1-s) spectral acceleration at 0.10 g, which are considered the threshold of damaging ground shaking levels. Again, we have averaged both of these ground motion types because that provides a more robust estimate of the potential damage. The potential damage probabilities from an earthquake in 2016 are particularly high in parts of north-central Oklahoma, northern Texas, southern Colorado/northern New Mexico, and north-central Arkansas. Some locations, such as small areas of Alabama and Mississippi, also show increased chance of damage from an earthquake in 2016 based on increased earthquake rates over the last few years. The hazard is also high over the New Madrid seismic zone, which experiences earthquakes at regular intervals (Petersen and others, 2014). These high chances of damage are similar to those found in parts of California (Petersen and others, 2014). The potential for damage from earthquakes near M6 (applied in this model) is consistent with other recent earthquakes: the Napa, Calif., M6.0 earthquake caused MMI of VIII (Did You Feel It?; U.S. Geological Survey, 2016d) or IX (ShakeMap; U.S. Geological Survey, 2016e); the Mineral, Virginia, M5.8 earthquake caused MMI of VII (Did You Feel It?; U.S. Geological Survey, 2016c); and the Prague, Okla., M5.6 earthquake caused MMI of VII (Did You Feel It?; U.S. Geological Survey, 2016b).

Conclusions

This report describes a 1-year seismic hazard assessment for the CEUS that includes induced and natural earthquakes. We developed two models for this purpose: (1) an informed model that depends mostly on the 1-year and 2-year earthquake catalogs as well as a discrimination between induced and natural earthquakes and (2) an adaptive model that considers the maximum earthquake rate in 1-year,

2-year, 36-year, and longer-term intervals and that does not discriminate between induced and natural earthquakes. Forecasts from these two hazard models are significantly higher than the 2014 NSHM by a factor of 3 or more. Generally, the two models agree within 50 percent or less from one another. The higher hazard levels in active injection areas could lead to potential damage across Oklahoma, Kansas, Colorado, New Mexico, Texas, and Arkansas. High hazard levels in some of these zones of induced seismicity are comparable with those in California and New Madrid, which also have high earthquake rates. Over the past decade, damage has already been observed at several locations in these states. However, some areas that have previously experienced induced earthquakes have quieted down over the past years, and the resulting hazard reverts back to what is portrayed in the 2014 National Seismic Hazard Model.

Further research from the science community on induced and natural earthquakes and their related ground shaking will improve these models. Future hazard models could be updated every year, or even over a shorter time period, to improve the model's predictability and its usefulness to policy makers. Varying disposal activities, policy changes, and further scientific research will change this model. The analysis could also be expanded to include induced earthquakes in the Western United States. Uncertainties are high in this analysis, and an important topic for future research is to try to quantify and reduce these uncertainties. Such efforts would be in line with Operational Earthquake Forecasting objectives that have been proposed for use by policy makers in decision making (Jordan and Jones, 2010; Field and others, 2016). Policy makers may consider these maps in formulating risk mitigation strategies.

References

Ake, Jon; Mahrer, Kenneth; O'Connell, Daniel; and Block, Lisa, 2005, Deep-injection and closely monitored induced seismicity at Paradox Valley, Colorado: Bulletin of the Seismological Society of America, v. 95, no. 2, p. 664–683, accessed autumn 2015 at http://dx.doi.org/10.1785/0120040072.

Andrews, R.D., and Holland, Austin, 2015, Statement on Oklahoma seismicity, April 21, 2015: Oklahoma Geological Survey, 2 p., accessed autumn 2015 at http://wichita.ogs.ou.edu/documents/OGS_Statement-Earthquakes-4-21-15.pdf.

Atkinson, G.M., 2015, Ground-motion prediction equation for small-to-moderate events at short hypocentral distances, with application to induced-seismicity hazards: Bulletin of the Seismological Society of America, v. 105, no. 2A, p. 981–992, accessed autumn 2015 at http://dx.doi.org/10.1785/0120140142.

Benz, H.M., McMahon, N.D., Aster, R.C., McNamara, D.E., and Harris, D.B., 2015, Hundreds of earthquakes per day—The 2014 Guthrie, Oklahoma, earthquake sequence: Seismological Research Letters, v. 86, no. 5, p. 1318–1325, accessed autumn 2015 at http://dx.doi.org/10.1785/0220150019.

Block, L.V., Wood, C.K., Yeck, W.L., and King, V.M., 2014, The 24 January 2013 ML 4.4 earthquake near Paradox, Colorado, and its relation to deep well injection: Seismological Research Letters, v. 85, no. 3, p. 609–624, accessed autumn 2015 at http://dx.doi.org/10.1785/0220130188.

Block, L.V., Wood, C.K., Yeck, W.L., and King, V.M., 2015, Induced seismicity constraints on subsurface geological structure, Paradox Valley, Colorado: Geophysical Journal International, v. 200, no. 2, p. 1170–1193, accessed autumn 2015 at http://dx.doi.org/10.1093/gji/ggu459.

Brodsky, E.E., and Lajoie, L.J., 2013, Anthropogenic seismicity rates and operational parameters at the Salton Sea Geothermal Field: Science, v. 341, no. 6145, p. 543–546, accessed winter 2016 at http://dx.doi.org/10.1126/science.1239213.

Buchanan, R.C., 2015, Increased seismicity in Kansas: The Leading Edge, v. 34, no. 6, p. 614–617, accessed autumn 2015 at http://dx.doi.org/10.1190/tle34060614.1.

Cornell, C.A., 1968, Engineering seismic risk analysis: Bulletin of the Seismological Society of America, v. 58, p. 1583–1606.
Cox, R.T., 1991, Possible triggering of earthquakes by underground waste disposal in the El Dorado, Arkansas area: Seismological Research Letters, v. 62, no. 2, p. 113–122, accessed autumn 2015 at http://srl.geoscienceworld.org/content/62/2/113.
Davis, S.D., and Frohlich, Cliff, 1993, Did (or will) fluid injection cause earthquakes?—Criteria for a rational assessment: Seismological Research Letters, v. 64, no. 3–4, p. 207–224, accessed autumn 2015 at http://srl.geoscienceworld.org/content/64/3-4/207.
Davis, S.D., and Pennington, W.D., 1989, Induced seismic deformation in the Cogdell oil field of west Texas: Bulletin of the Seismological Society of America, v. 79, no. 5, p. 1477–1494. [Also available at http://www.bssaonline.org/content/79/5/1477.]
Douglas, John; Edwards, Benjamin; Convertito, Vincenzo; Sharma, Nitin; Tramelli, Anna; Kraaijpoel, Dirk; Mena Cabrera, Banu; Maercklin, Nils; and Troise, Claudia, 2013, Predicting ground motion from induced earthquakes in geothermal areas: Bulletin of the Seismological Society of America, v. 103, no. 3, p. 1875–1897, accessed autumn 2015 at http://dx.doi.org/10.1785/0120120197.
Eberhart-Phillips, Donna, and Oppenheimer, D.H., 1984, Induced seismicity in the Geysers geothermal area, California: Journal of Geophysical Research–Solid Earth, v. 89, no. B2, p. 1191–1207, accessed autumn 2015 at http://dx.doi.org/10.1029/JB089iB02p01191.
Ellsworth, W.L., 2013, Injection-induced earthquakes: Science, v. 341, no. 6142, 7 p., accessed autumn 2015 at http://dx.doi.org/10.1126/science.1225942.
Evans, D.M., 1966, The Denver area earthquakes and the Rocky Mountain Arsenal disposal well: The Mountain Geologist, v. 3, p. 23–36.
Feng, Qiuchun, and Lees, J.M., 1998, Microseismicity, stress, and fracture in the Coso geothermal field, California: Tectonophysics, v. 289, no. 1, p. 221–238, accessed winter 2016 at http://dx.doi.org/10.1016/S0040-1951(97)00317-X.
Field, E.H., Jordan, T.H., Jones, L.M., Michael, A.J., Blanpied, M.L., and other workshop participants, 2016, The potential uses of operational earthquake forecasting: Seismological Research Letters, v. 87, no. 2A, 10 p., accessed winter 2016 at http://srl.geoscienceworld.org/content/early/2016/02/02/0220150174.full.
Frankel, A.D., 1995, Mapping seismic hazard in the Central and Eastern United States: Seismological Research Letters, v. 66, p. 8–21.
Friberg, P.A., Besana-Ostman, G.M., and Dricker, Ilya, 2014, Characterization of an earthquake sequence triggered by hydraulic fracturing in Harrison County, Ohio: Seismological Research Letters, v. 85, no. 6, p. 1295–1307, accessed autumn 2015 at http://dx.doi.org/10.1785/0220140127.
Frohlich, Cliff, 2012, Two-year survey comparing earthquake activity and injection-well locations in the Barnett Shale, Texas: Proceedings of the National Academy of Sciences, v. 109, no. 35, p. 13934–13938, accessed autumn 2015 at http://dx.doi.org/10.1073/pnas.1207728109.
Frohlich, Cliff, and Brunt, Michael, 2013, Two-year survey of earthquakes and injection/production wells in the Eagle Ford Shale, Texas, prior to the Mw4.8 20 October 2011 earthquake: Earth and Planetary Science Letters, v. 379, p. 56–63, accessed autumn 2015 at http://dx.doi.org/10.1016/j.epsl.2013.07.025.
Frohlich, Cliff; Ellsworth, William; Brown, W.A.; Brunt, Michael; Luetgert, Jim; MacDonald, Tim; and Walter, Steve, 2014, The 17 May 2012 M4.8 earthquake near Timpson, east Texas—An event possibly triggered by fluid injection: Journal of Geophysical Research–Solid Earth, v. 119, no. 1, p. 581–593, accessed autumn 2015 at http://dx.doi.org/10.1002/2013JB010755.

Frohlich, Cliff; Glidewell, Jennifer; and Brunt, Michael, 2012, Location and felt reports for the 25 April 2010 mbLg 3.9 earthquake near Alice, Texas—Was it induced by petroleum production?: Bulletin of the Seismological Society of America, v. 102, no. 2, p. 457–466, accessed autumn 2015 at http://dx.doi.org/10.1785/0120110179.

Frohlich, Cliff; Hayward, Chris; Stump, Brian; and Potter, Eric, 2011, The Dallas-Fort Worth earthquake sequence—October 2008 through May 2009: Bulletin of the Seismological Society of America, v. 101, no. 1, p. 327–340, accessed autumn 2015 at http://dx.doi.org/10.1785/0120100131.

Frohlich, Cliff, Walter, J.I., and Gale, J.F.W, 2015, Analysis of transportable array (USArray) data shows earthquakes are scarce near injection wells in the Williston Basin, 2008–2011: Seismological Research Letters, v. 86, no. 2A, p. 492–499, accessed autumn 2015 at http://dx.doi.org/10.1785/0220140180.

Gan, Wei, and Frohlich, Cliff, 2013, Gas injection may have triggered earthquakes in the Cogdell oil field, Texas: Proceedings of the National Academy of Sciences, v. 110, no. 47, p. 18786–18791, accessed autumn 2015 at http://dx.doi.org/10.1073/pnas.1311316110.

Gardner, J.K., and Knopoff, Leon, 1974, Is the sequence of earthquakes in southern California, with aftershocks removed, Poissonian?: Bulletin of the Seismological Society of America, v. 64, no. 5, p. 1363–1367.

Gomberg, Joan, and Wolf, Lorraine, 1999, Possible cause for an improbable earthquake—The 1997 MW 4.9 southern Alabama earthquake and hydrocarbon recovery: Geology, v. 27, no. 4, p. 367–370, accessed autumn 2015 at http://dx.doi.org/10.1130/0091-7613(1999)027<0367:PCFAIE>2.3.CO;2.

Ground Water Protection Council and Interstate Oil and Gas Compact Commission, 2015, Potential injection-induced seismicity associated with oil & gas development—A primer on technical and regulatory considerations informing risk management and mitigation: Ground Water Protection Council and Interstate Oil and Gas Compact Commission, 141 p., accessed autumn 2015 at http://www.gwpc.org/sites/default/files/finalprimerweb.pdf.

Gutenberg, Beno, and Richter, C.F., 1944, Frequency of earthquakes in California: Bulletin of the Seismological Society of America, v. 34, no. 4, p.185–188.

Hauksson, Egill; Göbel, Thomas; Ampuero, J.-P.; and Cochran, Elizabeth, 2015, A century of oil-field operations and earthquakes in the greater Los Angeles Basin, southern California: The Leading Edge, v. 34, no. 6, p. 650–656, accessed autumn 2015 at http://dx.doi.org/10.1190/tle34060650.1.

Healy, J.H., Rubey, W.W., Griggs, D.T., and Raleigh, C.B., 1968, The Denver earthquakes: Science, v. 161, no. 3848, 10 p., accessed autumn 2015 at http://prod-earthquake.cr.usgs.gov/research/induced/pdf/Healy-et-al-1968-Science-(New-York-NY).pdf.

Hornbach, M.J., DeShon, H.R., Ellsworth, W.L., Stump, B.W., Hayward, Chris, Frohlich, Cliff, Oldham, H.R., Olson, J.E., Magnani, M.B., Brokaw, Casey, and Luetgert, J.H., 2015, Causal factors for seismicity near Azle, Texas: Nature Communications, v. 6, 11 p., accessed autumn 2015 at http://dx.doi.org/10.1038/ncomms7728.

Horton, Steve, 2012, Disposal of hydrofracking waste fluid by injection into subsurface aquifers triggers earthquake swarm in central Arkansas with potential for damaging earthquake: Seismological Research Letters, v. 83, no. 2, p. 250–260, accessed autumn 2015 at http://dx.doi.org/10.1785/gssrl.83.2.250.

Hough, S.E., 2014, Shaking from injection-induced earthquakes in the Central and Eastern United States: Bulletin of the Seismological Society of America, v. 104, p. 2619–2626, accessed autumn 2015 at http://dx.doi.org/10.1785/0120140099.

Hough, S.E., and Page, Morgan, 2015, A century of induced earthquakes in Oklahoma?: Bulletin of the Seismological Society of America, v. 105, no. 6, p. 2863–2870, accessed autumn 2015 at http://dx.doi.org/10.1785/0120150109.

Jordan, T.H., and Jones, L.M., 2010, Operational earthquake forecasting—Some thoughts on why and how: Seismological Research Letters, v. 81, no. 4, p. 571–574.

Justinic, A.H.; Stump, Brian; Hayward, Chris; and Frohlich, Cliff, 2013, Analysis of the Cleburne, Texas, earthquake sequence from June 2009 to June 2010: Bulletin of the Seismological Society of America, v. 103, no. 6, p. 3083–3093, accessed autumn 2015 at http://dx.doi.org/10.1785/0120120336.

Keranen, K.M., Savage, H.M., Abers, G.A., and Cochran E.S., 2013, Potentially induced earthquakes in Oklahoma, USA—Links between wastewater injection and the 2011 Mw 5.7 earthquake sequence: Geology, v. 41, no. 6, p. 699–702, accessed autumn 2015 at http://dx.doi.org/10.1130/G34045.1.

Keranen, K.M., Weingarten, Matthew, Abers, G.A., Bekins, B.A., and Ge, Shemin, 2014, Sharp increase in central Oklahoma seismicity since 2008 induced by massive wastewater injection: Science, v. 345, no. 6195, p. 448–451, accessed autumn 2015 at http://dx.doi.org/10.1126/science.1255802.

Kim, W.-Y., 2013, Induced seismicity associated with fluid injection into a deep well in Youngstown, Ohio: Journal of Geophysical Research–Solid Earth, v. 118, no. 7, p. 3506–3518, accessed autumn 2015 at http://dx.doi.org/10.1002/jgrb.50247.

King, V.M., Block, L.V., Yeck, W.L., Wood, C.K., and Derouin, S.A., 2014, Geological structure of the Paradox Valley Region, Colorado, and relationship to seismicity induced by deep well injection: Journal of Geophysical Research–Solid Earth, v. 119, no. 6, p. 4955–4978, accessed autumn 2015 at http://dx.doi.org/10.1002/2013JB010651.

Llenos, A.L., and Michael, A.J., 2013, Modeling earthquake rate changes in Oklahoma and Arkansas—Possible signatures of induced seismicity: Bulletin of the Seismological Society of America, v. 103, no. 5, p. 2850–2861, accessed autumn 2015 at http://dx.doi.org/10.1785/0120130017.

Llenos, Andrea; Ellsworth, William; and Michael, Andrew, 2015, Earthquake rate models for evolving induced seismicity hazard in the Central and Eastern U.S. [abs.], *in* American Geophysical Union Fall Meeting, San Francisco, Calif., December 14–18, 2015, Proceedings: American Geophysical Union, abstract S21C-03. [Also available at https://agu.confex.com/agu/fm15/meetingapp.cgi/Paper/67871.]

McGarr, Arthur, 2014, Maximum magnitude earthquakes induced by fluid injection: Journal of Geophysical Research–Solid Earth, v. 119, no. 2, p. 1008–1019, accessed autumn 2015 at http://dx.doi.org/10.1002/2013JB010597.

McGarr, Arthur; Bekins, Barbara; Burkardt, Nina; Dewey, James; Earle, Paul; Ellsworth, William; Ge, Shemin; Hickman, Stephen; Holland, Austin; Majer, Ernest; Rubinstein, Justin; and Sheehan, Anne, 2015, Coping with earthquakes induced by fluid injection: Science, v. 347, no. 6224, p. 830–831, accessed autumn 2015 at http://dx.doi.org/10.1126/science.aaa0494.

McNamara, D.E.; Benz, H.M.; Herrmann, R.B.; Bergman, E.A.; Earle, Paul; Holland, Austin; Baldwin, Randy; and Gassner, A., 2015a, Earthquake hypocenters and focal mechanisms in central Oklahoma reveal a complex system of reactivated subsurface strike-slip faulting: Geophysical Research Letters, v. 42, no. 8, p. 2742–2749, accessed autumn 2015 at http://dx.doi.org/10.1002/2014GL062730.

McNamara, D.E.; Hayes, G.P.; Benz, H.M.; Williams, R.A.; McMahon, N.D.; Aster, R.C.; Holland, Austin; Sickbert, Timothy; Herrmann, Robert; Briggs, Richard; Smoczyk, Gregory; Bergman, Eric; and Earle, Paul, 2015b, Reactivated faulting near Cushing, Oklahoma—Increased potential for a triggered earthquake in an area of United States strategic infrastructure: Geophysical Research

Letters, v. 42, no. 20, p. 8328–8332, accessed autumn 2015 at http://dx.doi.org/10.1002/2015GL064669.
Meremonte, M.E., Lahr, J.C., Frankel, A.D., Dewey, J.W., Crone, A.J., Overturf, D.E., Carver, D.L., and Bice, W.T., 2001, Investigation of an earthquake swarm near Trinidad, Colorado, August–October 2001: U.S. Geological Survey Open-File Report 02–0073, accessed autumn 2015 at http://pubs.usgs.gov/of/2002/ofr-02-0073/ofr-02-0073.html.
Nicholson, Craig; Roeloffs, Evelyn; and Wesson, R.L., 1988, The northeastern Ohio earthquake of 31 January 1986—Was it induced?: Bulletin of the Seismological Society of America, v. 78, no. 1, p. 188–217, accessed autumn 2015 at http://bssa.geoscienceworld.org/content/78/1/188.
Oppenheimer, D.H., 1986, Extensional tectonics at the Geysers geothermal area, California: Journal of Geophysical Research–Solid Earth, v. 91, no. B11, p. 11463–11476, accessed autumn 2015 at http://dx.doi.org/10.1029/JB091iB11p11463.
Pennington, W.D., Davis, S.D., Carlson, S.M., DuPree, James, and Ewing, T.E., 1986, The evolution of seismic barriers and asperities caused by the depressuring of fault planes in oil and gas fields of south Texas: Bulletin of the Seismological Society of America, v. 76, no. 4, p. 939–948. [Also available at http://www.bssaonline.org/content/76/4/939.]
Petersen, M.D., Moschetti, M.P., Powers, P.M., Mueller, C.S., Haller, K.M., Frankel, A.D., Zeng, Yuehua, Rezaeian, Sanaz, Harmsen, S.C., Boyd, O.S., Field, Ned, Chen, Rui, Rukstales, K.S., Luco, Nico, Wheeler, R.L., Williams, R.A., and Olsen, A.H., 2014, Documentation for the 2014 update of the United States National Seismic Hazard Maps: U.S. Geological Survey Open-File Report 2014–1091, 243 p., accessed autumn 2015 at http://dx.doi.org/10.3133/ofr20141091.
Petersen, M.D., Moschetti, M.P., Powers, P.M., Mueller, C.S., Haller, K.M., Frankel, A.D., Zeng, Yuehua, Rezaeian, Sanaz, Harmsen, S.C., Boyd, O.S., Field, Ned, Chen, Rui, Rukstales, K.S., Luco, Nico, Wheeler, R.L., Williams, R.A., and Olsen, A.H., 2015a, The 2014 United States National Seismic Hazard Model: Earthquake Spectra, v. 31, no. S1, p. S1–S30, accessed autumn 2015 at http://dx.doi.org/10.1193/120814EQS210M.
Petersen, M.D., Mueller, C.S., Moschetti, M.P., Hoover, S.M., Rubinstein, J.L., Llenos, A.L., Michael, A.J., Ellsworth, W.L., McGarr, A.F., Holland, A.A., and Anderson, J.G., 2015b, Incorporating induced seismicity in the 2014 United States National Seismic Hazard Model—Results of 2014 workshop and sensitivity studies: U.S. Geological Survey Open-File Report 2015–1070, 69 p., accessed autumn 2015 at http://dx.doi.org/10.3133/ofr20151070.
Pursley, Jana, Bilek, S.L., and Ruhl, C.J., 2013, Earthquake catalogs for New Mexico and bordering areas, 2005–2009: New Mexico Geology, v. 35, no. 1, p. 3–12. [Also available at https://geoinfo.nmt.edu/publications/periodicals/nmg/35/n1/nmg_v35_n1_p3.pdf.]
Raleigh, C.B., Healy, J.H., and Bredehoeft, J.D., 1976, An experiment in earthquake control at Rangely, Colorado: Science, v. 191, no. 4233, p. 1230–1237, accessed autumn 2015 at http://dx.doi.org/10.1126/science.191.4233.1230.
Rothe, G.H., and Lui, C.-Y., 1983, Possibility of induced seismicity in the vicinity of the Sleepy Hollow oil field, southwestern Nebraska: Bulletin of the Seismological Society of America, v. 73, no. 5, p. 1357–1367. [Also available at http://www.bssaonline.org/content/73/5/1357.]
Rubinstein, J.L., Ellsworth, W.L, McGarr, Arthur, and Benz, H.M., 2014, The 2001–present induced earthquake sequence in the Raton Basin of northern New Mexico and southern Colorado: Bulletin of the Seismological Society of America, v. 104, no. 5, p. 2162–2181, accessed autumn 2015 at http://dx.doi.org/10.1785/0120140009.
Sanford, Allan; Balch, Robert; Jaksha, Lawrence; and Delap Susan, 1993, Location and fault mechanism of the 2 January 1992 Rattlesnake Canyon earthquake in southeastern New Mexico: New

Mexico Institute of Mining and Technology Geophysics Open-File Report 70, 11 p., accessed autumn 2015 at http://www.ees.nmt.edu/images/ees/Geop/nmquakes/R70/R70.HTM.
Sanford, A.R., Mayeau, T.M., Schlue, J.W., Aster, R.C., and Jaksha, L.H., 2006, Earthquake catalogs for New Mexico and bordering areas II, 1999–2004: New Mexico Geology, v. 28, p. 99–109.
Seeber, Leonardo, Armbruster, J.G., and Kim, W.-Y., 2004, A fluid-injection triggered earthquake sequence in Ashtabula, Ohio—Implications for seismogenesis in stable continental regions: Bulletin of the Seismological Society of America, v. 94, no. 1, p. 76–87, accessed autumn 2015 at http://dx.doi.org/10.1785/0120020091.
Segall, Paul, 1989, Earthquakes triggered by fluid extraction: Geology, v. 17, no. 10, p. 942–946, accessed winter 2016 at http://geology.gsapubs.org/content/17/10/942.
Segall, Paul, and Lu, S., 2015, Injection-induced seismicity—Poroelastic and earthquake nucleation effects: Journal of Geophysical Research–Solid Earth, v. 120, no. 7, p. 5082–5103, accessed winter 2016 at http://dx.doi.org/10.1002/2015JB012060.
Skoumal, R.J., Brudzinski, M.R., and Currie, B.S., 2015a, Distinguishing induced seismicity from natural seismicity in Ohio—Demonstrating the utility of waveform template matching: Journal of Geophysical Research–Solid Earth, v. 120, no. 9, p. 6284–6296, accessed autumn 2015 at http://dx.doi.org/10.1002/2015JB012265.
Skoumal, R.J., Brudzinski, M.R., and Currie, B.S., 2015b, Earthquakes induced by hydraulic fracturing in Poland Township, Ohio: Bulletin of the Seismological Society of America, v. 105, no. 1, p. 189–197, accessed autumn 2015 at http://dx.doi.org/10.1785/0120140168.
Smith, Bill; Beall, Joseph; and Stark, Mitchel, 2000, Induced seismicity in the SE Geysers field, California, USA, *in* World Geothermal Congress 2000, Kyushu-Tohoku, Japan, May 28–June 10, 2000, Proceedings: International Geothermal Association, p. 2887–2892. [Also available at http://www.geothermal-energy.org/pdf/IGAstandard/WGC/2000/R0579.PDF]
Stewart, J.P., and Seyhan, Emel, 2013, Semi-empirical nonlinear site amplification and its application in NEHRP site factors: Berkeley, Calif., Pacific Earthquake Engineering Research Center, PEER Report 13, 59 p.
Sumy, D.F., Cochran, E.S., Keranen, K.M., Wei, Maya, and Abers, G.A., 2014, Observations of static Coulomb stress triggering of the November 2011 M5.7 Oklahoma earthquake sequence: Journal of Geophysical Research–Solid Earth, v. 119, no. 3, 1904–1923, accessed winter 2016 at http://dx.doi.org/10.1002/2013JB010612.
U.S. Energy Information Administration, 2015, Maps—Exploration, resources, reserves, and production. Oil and gas field data in Shapefile format: U.S. Energy Information Administration Web page, accessed summer 2015 at https://www.eia.gov/pub/oil_gas/natural_gas/analysis_publications/maps/maps.htm.
U.S. Geological Survey, 2016a, M4.2—6km ENE of Edmond, Oklahoma. Impact—ShakeMap: U.S. Geological Survey Web page, accessed winter 2016 at http://earthquake.usgs.gov/earthquakes/eventpage/us10004aqg#impact_shakemap.
U.S. Geological Survey, 2016b, M5.6—Oklahoma. Impact—Did You Feel It?: U.S. Geological Survey Web page, accessed winter 2016 at http://earthquake.usgs.gov/earthquakes/eventpage/usp000jadn#impact_dyfi.
U.S. Geological Survey, 2016c, M5.8—Virginia. Impact—Did You Feel It?: U.S. Geological Survey Web page, accessed winter 2016 at http://earthquake.usgs.gov/earthquakes/eventpage/usp000j6xc#impact_dyfi.

U.S. Geological Survey, 2016d, M6.0— 6km NW of American Canyon, California. Impact—Did You Feel It?: U.S. Geological Survey Web page, accessed winter 2016 at http://earthquake.usgs.gov/earthquakes/eventpage/nc72282711#impact_dyfi.
U.S. Geological Survey, 2016e, M6.0— 6km NW of American Canyon, California. Impact—ShakeMap: U.S. Geological Survey Web page, accessed winter 2016 at http://earthquake.usgs.gov/earthquakes/eventpage/nc72282711#impact_shakemap.
Wald, D.J., and Allen, T.I., 2007, Topographic slope as a proxy for seismic site conditions and amplification: Bulletin of the Seismological Society of America, v. 97, no. 5, p. 1379–1395, accessed autumn 2015 at http://dx.doi.org/10.1785/0120060267.
Wald, D.J., Quitoriano, Vincent, Worden, C.B., Hopper, Margaret, and Dewey, J.W., 2011, USGS "Did You Feel It?" Internet-based macroseismic intensity maps: Annals of Geophysics, v. 54, no. 6, p. 688–707, accessed autumn 2015 at http://dx.doi.org/10.4401/ag-5354.
Walsh, F.R., and Zoback, M.D., 2015, Oklahoma's recent earthquakes and saltwater disposal: Science Advances, v. 1, no. 5, e1500195, 9 p., accessed autumn 2015 at http://dx.doi.org/10.1126/sciadv.1500195.
Wei, Shengji; Avouac, J.-P.; Hudnut, K.W.; Donnellan, Andrea; Parker, J.W.; Graves, R.W.; Helmberger, Don; Fielding, Eric; Liu, Zhen; Cappa, Frederic; and Eneva, Mariana, 2015, The 2012 Brawley swarm triggered by injection-induced aseismic slip: Earth and Planetary Science Letters, v. 422, p. 115–125, accessed autumn 2015 at http://dx.doi.org/10.1016/j.epsl.2015.03.054.
Weingarten, Matthew, Ge, Shemin, Godt, J.W., Bekins, B.A., and Rubinstein, J.L., 2015, High-rate injection is associated with the increase in U.S. mid-continent seismicity: Science, v. 348, no. 6241, p. 1336–1340, accessed autumn 2015 at http://dx.doi.org/10.1126/science.aab1345.
Wesson, R.L., and Nicholson, Craig, 1987, Earthquake hazard associated with deep well injection—A report to the U.S. Environmental Protection Agency: U.S. Geological Survey Open-File Report 87–331, 111 p., accessed autumn 2015 at https://pubs.er.usgs.gov/publication/ofr87331.
Worden, C.B., Wald, D.J., Lin, Kuo-wan, Garcia, Daniel, and Cua, Georgia, 2010, A revised ground-motion and intensity interpolation scheme for ShakeMap: Bulletin of the Seismological Society of America, v. 100, no. 6, p. 3083–3096, accessed autumn 2015 at http://dx.doi.org/10.1785/0120100101.
Yeck, W.L., Block, L.V., Wood, C.K., and King, V.M., 2015, Maximum magnitude estimations of induced earthquakes at Paradox Valley, Colorado, from cumulative injection volume and geometry of seismicity clusters: Geophysical Journal International, v. 200, no. 1, p. 322–336, accessed autumn 2015 at http://dx.doi.org/10.1093/gji/ggu394.
Yeck, William; Sheehan, Anne; Weingarten, Matthew; and Nakai, Jenny, 2014, The 2014 Weld County, Colorado, earthquakes—A developing case of induced seismicity? [abs.], *in* American Geophysical Union Fall Meeting, San Francisco, Calif., December 15–19, 2014, Proceedings: American Geophysical Union, abstract S51A-4393. [Also available at https://agu.confex.com/agu/fm14/meetingapp.cgi/Paper/29513.]

Appendix 1. Likelihood Testing for Smoothed Seismicity Parameters, Oklahoma and Southern Kansas

Smoothing parameters for the earthquake rate models are informed by likelihood testing of the smoothing distance and catalog duration and timing. Details about the likelihood calculations are provided elsewhere (Moschetti, 2015); here, we only summarize those results. Likelihood testing employs trial earthquake rate models developed by varying the smoothing distance and time period for computing the smoothed seismicity models. All smoothed seismicity models were developed with isotropic, Gaussian smoothing kernels, where the smoothing distance represents the kernel width. Likelihood testing was only carried out for the earthquakes occurring in the Oklahoma-Kansas zone of induced seismicity (fig. 1, table 1) because other zones contained too few events for the statistical analysis.

Likelihood testing follows previous work (for example, Werner and others, 2010; Moschetti, 2015) by comparing trial smoothed seismicity models with independent sets of later-occurring earthquakes ("testing catalogs"). Likelihood values derive from Poisson probabilities and follow a rate-normalized formulation that provides information about the spatial distribution of seismicity only (Werner and others, 2010). Trial rate models were developed from smoothing distances of 5 kilometers (km), 10 km, 15 km, 20 km, 25 km, 35 km, 50 km, 75 km, and 100 km, and from events occurring in 1-year time periods from calendar years 2009 through 2014. Likelihood of the smoothed seismicity models was computed from moment magnitude (M) ≥2.5 and M≥3.5 earthquakes from the period January–June 2015. Likelihood values are presented as the per-earthquake information gain achieved from the use of the smoothed seismicity model compared to the use of a uniform-rate model with the zone of induced seismicity.

Information gains from the likelihood testing are summarized in figure 1–1. Maximum information gains are achieved from the use of earthquakes occurring in 2014. The corresponding smoothing distance for this smoothed seismicity model is developed from a 10-km smoothing distance. Because of error bounds on the information gain estimates, we characterize the 10- and 20-km smoothing distances as optimized smoothing distances (Rhoades and others, 2011).

Development of the induced-earthquake rate models employs the main scientific findings of this likelihood testing. For the informed model (see the text of this report for details), most weight (0.90) within zones of induced seismicity is applied to the logic tree branch for the 1-year earthquake catalog. Equal weight (0.50) is applied to smoothing distances of 10 km and 20 km within the induced seismicity zones.

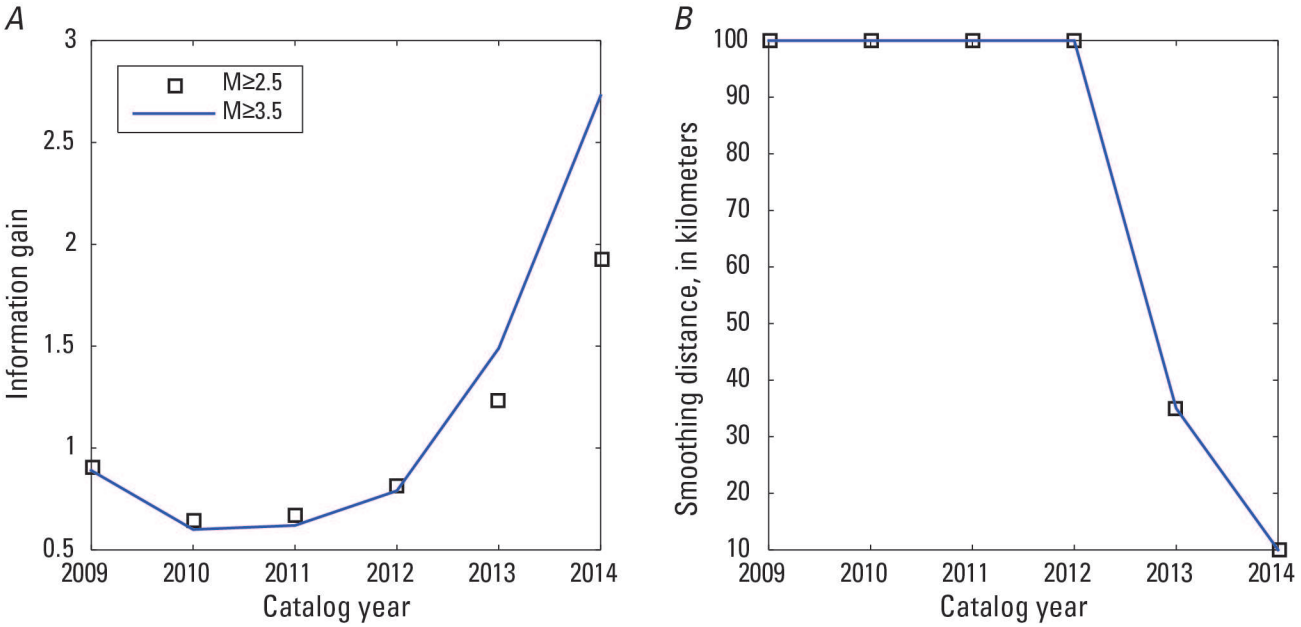

Figure 1–1. Information gains (*A*) and optimized smoothing distances (*B*) as a function of the catalog year of the events used to develop trial smoothed seismicity models. Results from moment magnitude (M) ≥2.5 and M≥3.5 earthquakes are identified by the explanation in fig. 1–1*A*.

References

Moschetti, M.P., 2015, A long-term earthquake rate model for the Central and Eastern United States from smoothed seismicity: Bulletin of the Seismological Society of America, v. 105, no. 6, p. 2928–2941. [Also available at http://dx.doi.org/10.1785/0120140370.]

Rhoades, D.A., Schorlemmer, Danijel, Gerstenberger, M.C., Christophersen, Annemarie, Zechar, J.D., and Imoto, Masajiro, 2011, Efficient testing of earthquake forecasting models: Acta Geophysica, v. 59, no. 4, p. 728–747. [Also available at http://www.degruyter.com/view/j/acgeo.2011.59.issue-4/s11600-011-0013-5/s11600-011-0013-5.xml.]

Werner, M.J., Helmstetter, Agnes, Jackson, D.D., and Kagan, Y.Y., 2011, High-resolution long-term and short-term earthquake forecasts for California: Bulletin of the Seismological Society of America, v. 101, no. 4, p. 1630–1648. [Also available at http://dx.doi.org/10.1785/0120090340.]

Appendix 2. The Adaptive Model

In this appendix, we provide further details about the adaptive model, an alternative earthquake rate model in which we assume that we cannot distinguish between natural and induced earthquakes. Rather than basing the 2016 one-year forecast on earthquake rates estimated over a single time window, the adaptive model compares earthquake rates over multiple time windows (1-year, 2-year, and 36-year durations) and uses the maximum of these rates only if it is significantly greater than the rates of the long-term 2014 National Seismic Hazard Model (NSHM). Otherwise, the long-term 2014 NSHM rate is used. In each spatial grid cell, we computed the rates of earthquakes of moment magnitude (M) 2.7 or greater in the declustered catalog over the three different time windows. The rates were obtained by spatially smoothing the earthquake counts over each time period with a Gaussian kernel using a 10-kilometer (km) correlation distance for the 1-year rate, a 20-km distance for the 2-year rate, and a 50-km distance for the 36-year rate. However, single mainshocks that happen to occur in these smaller time windows may raise the short-term rates far above the long-term 2014 NSHM rate and yet may not be unexpected given the long-term rate model. To minimize the effect of this type of fluctuation, we have developed the following trimming strategy. If the number of earthquakes within some specified trimming distance of a grid cell over either the 1-year, 2-year, or 36-year time period does not exceed the expected number given the long-term 2014 NSHM at the 95-percent confidence level, then we simply use the 2014 NSHM rate in that cell. At present, the trimming distance is set to match the changes we implement in the spatial smoothing kernel over time (for example, the trimming distance is 50 km for the 36-year window, 20 km for the 2-year window, and 10 km for the 1-year window) and in general should reflect the improvement in earthquake location accuracy over time. Figure 2–1 demonstrates the effect of this trimming strategy. When trimming is not applied, there are many small areas that have a high maximum rate simply because of isolated mainshocks temporarily increasing the short-term rate above the long-term (fig. 2–1*A*). Trimming masks out these areas, limiting the higher maximum rates to the areas with rates that are significantly greater than the long-term 2014 NSHM rate (fig. 2–1*B*). Figure 2–1*C* identifies the earthquakes that remain after the trimming. Figure 2–2 compares the trimmed and untrimmed rates using difference and ratio maps. The adaptive model therefore essentially consists of the maximum rate from among the trimmed earthquake rates from the three time windows and the earthquake rate from the 2014 NSHM (fig. 2–1*B*).

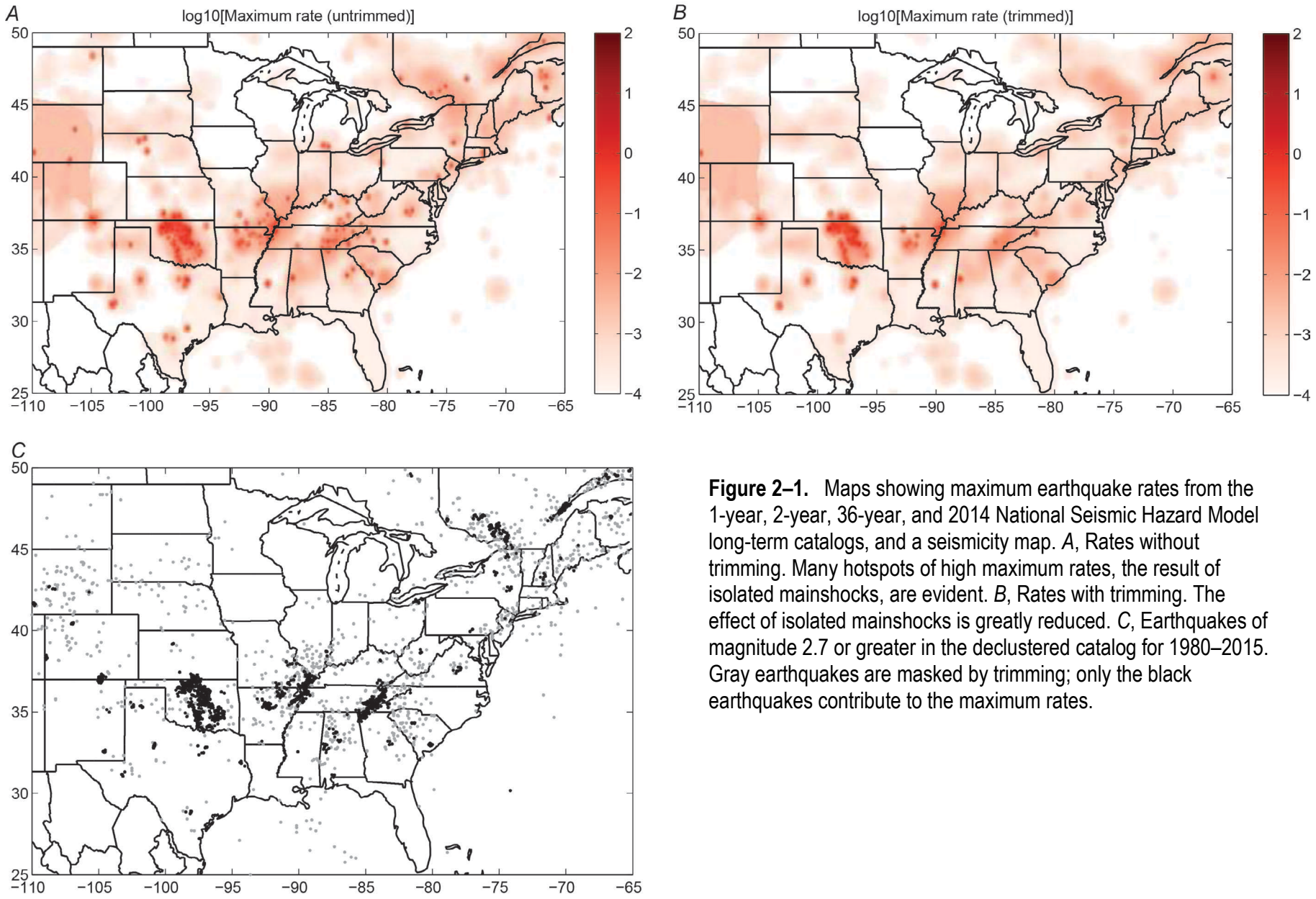

Figure 2–1. Maps showing maximum earthquake rates from the 1-year, 2-year, 36-year, and 2014 National Seismic Hazard Model long-term catalogs, and a seismicity map. *A*, Rates without trimming. Many hotspots of high maximum rates, the result of isolated mainshocks, are evident. *B*, Rates with trimming. The effect of isolated mainshocks is greatly reduced. *C*, Earthquakes of magnitude 2.7 or greater in the declustered catalog for 1980–2015. Gray earthquakes are masked by trimming; only the black earthquakes contribute to the maximum rates.

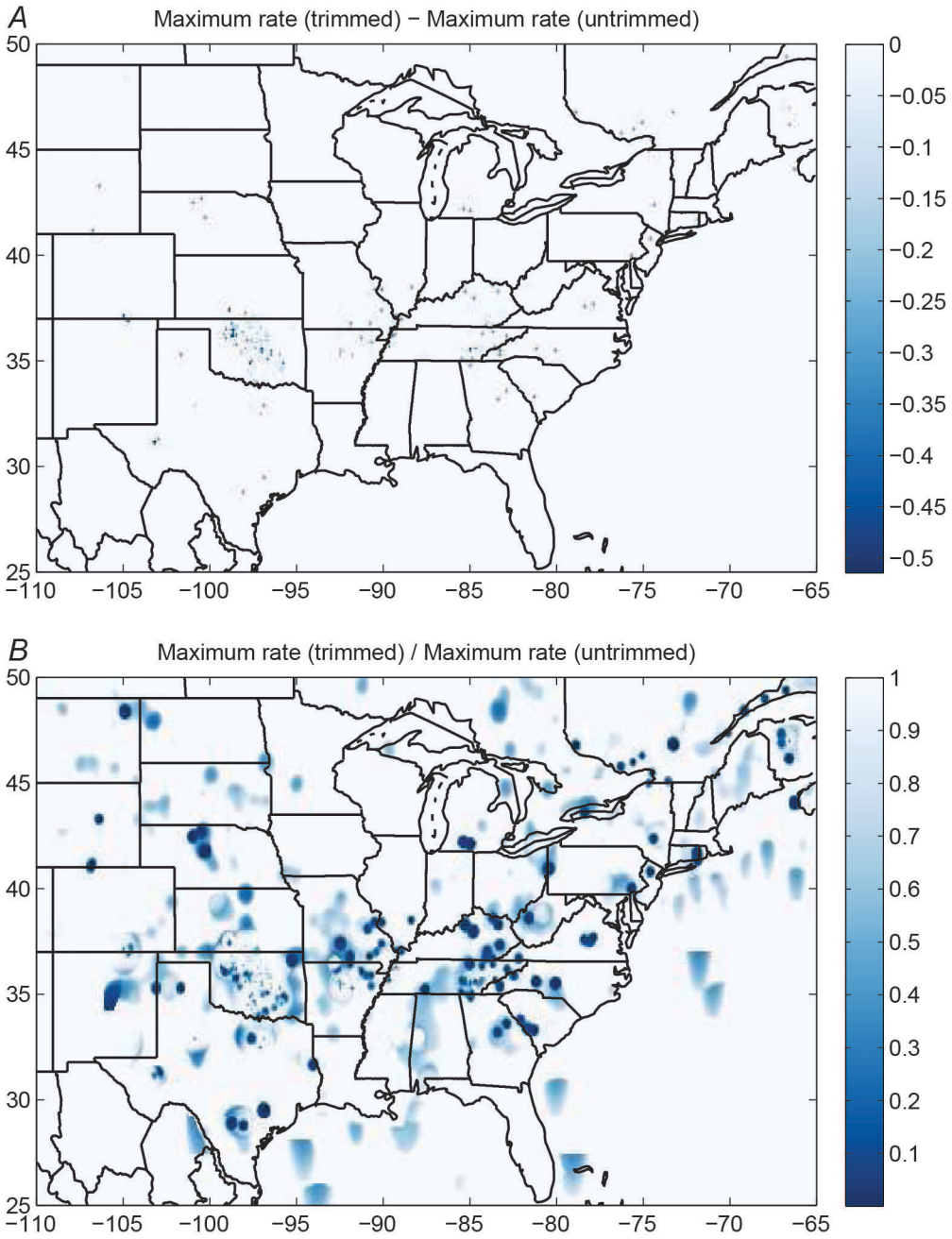

Figure 2–2. Maps comparing trimmed and untrimmed earthquake rates. *A*, Difference of trimmed rates minus untrimmed rates. *B*, Ratio of trimmed rates over untrimmed rates.

ISSN 2331-1258 (online)
http://dx.doi.org/10.3133/ofr20161035